Research Square

Preprints are preliminary reports that have not undergone peer review.
They should not be considered conclusive, used to inform clinical practice,
or referenced by the media as validated information.

Rare Fungal Diversity in NASA Mars 2020 Mission Assembly Environments Revealed by Six Novel Species and Comparative Functional Genomics

Atul Chander
Jet Propulsion Laboratory
Anna Tumeo
University of Galway
Nitin Kumar Singh
Jet Propulsion Laboratory
Enos Jadin
Indian Institute of Technology Madras
Michael P. Williams
Jet Propulsion Laboratory
Dongwook Kim
University of Lausanne
Gustavo Soares
Universidade de Brasília
Marcus de Melo Teixeira
Universidade de Brasília
Georgios Miliotis
University of Galway
Christopher E. Mason
Weill Cornell Medicine
Tamas Torok
Lawrence Berkeley National Laboratory
Kasthuri Venkateswaran
kjvenkat1955@gmail.com

Jet Propulsion Laboratory

Article

Keywords: spacecraft assembly cleanrooms, Mars 2020, fungal diversity, novel fungal species, integrative taxonomy, multilocus phylogeny, comparative genomics, planetary protection

Posted Date: November 12th, 2026

DOI: https://doi.org/10.21203/rs.3.rs-11459298/v1

License: This work is licensed under a Creative Commons Attribution 4.0 International License.
Read Full License

Additional Declarations:
No competing interests reported.

Tables are available in the Supplementary Files section

Rare Fungal Diversity in NASA Mars 2020 Mission Assembly Environments Revealed by Six Novel Species and Comparative Functional Genomics

Atul Munish Chander[1,2$], Anna Tumeo[3$], Nitin Kumar Singh[1,4$], Enos Jadin[5], Michael P. Williams[1], Dongwook Kim[6,7], Gustavo Soares[8], Marcus de Melo Teixeira[8], Georgios Miliotis[3], Christopher E. Mason[9*], Tamas Torok[10], and Kasthuri Venkateswaran[1,11*]

Affiliations:

1. Jet Propulsion Laboratory, California Institute of Technology, M/S 89-2, 4800 Oak Grove Dr., Pasadena, CA 91109, USA
2. Department of Biology, University of Mississippi, University, MS 38677, USA
3. Antimicrobial Resistance and Microbial Ecology Group, School of Medicine, University of Galway, Galway, H91 TK33, Ireland
4. Department of Industrial Relations, Division of Occupational Safety and Health, Oakland, CA 94611, USA
5. Department of Biotechnology, Bhupat and Jyoti Mehta School of Biosciences, Indian Institute of Technology-Madras, Chennai, Tamil Nadu, 600036, India
6. Department of Computational Biology, University of Lausanne, 1015 Lausanne, Switzerland
7. SIB Swiss Institute of Bioinformatics, 1015 Lausanne, Switzerland
8. School of Medicine, University of Brasilia, Brasilia 70910-900, Brazil
9. Department of Physiology and Biophysics and the WorldQuant Initiative for Quantitative Prediction, Weill Cornell Medicine, New York, NY 10021, USA
10. Lawrence Berkeley National Laboratory, Ecology Department, Berkeley, CA 94720, USA
11. Department of Space Studies, University of North Dakota, Grand Forks, ND 58202, USA

[$]These authors contributed equally to this work and shared first authorship.

*Authors for correspondence:

(A) Kasthuri Venkateswaran, kjvenkat1955@gmail.com, +1 626 833 2122

(B) Christopher Mason, christopher.e.mason@gmail.com

Authors' email and ORCID#:

1. Atul Chander: amchander@gmail.com; https://orcid.org/0000-0001-9582-6638
2. Anna Tumeo: a.tumeo1@universityofgalway.ie; https://orcid.org/0009-0007-7689-2809
3. Nitin Singh: mail2nitinks@gmail.com
4. Enos Jadin: enosjadlin007@gmail.com
5. Michael Williams: mpw550@gmail.com
6. Dongwook Kim: endix1029@gmail.com; https://orcid.org/0000-0001-7386-3163
7. Gustavo Soares: gusta.soaresaraujo@gmail.com
8. Marcus de Melo Teixeira: marcus.teixeira@gmail.com
9. Georgios Miliotis: georgios.miliotis@universityofgalway.ie; https://orcid.org/0000-0002-0944-2206
10. Christopher Mason: christopher.e.mason@gmail.com
11. Tamas Torok: ttorok@lbl.gov; https://orcid.org/0000-0002-6895-6936
12. Kasthuri Venkateswaran: kjvenkat1955@gmail.com; https://orcid.org/0000-0002-6742-0873

Running title: Rare fungi from Mars 2020 assembly environments

Abstract

NASA cleanrooms are oligotrophic, low-biomass environments maintained under stringent contamination-control procedures, yet they continuously yield formerly uncharacterized fungi. Here, we examined seven isolates recovered from Jet Propulsion Laboratory and Kennedy Space Center facilities during assembly of the Mars 2020 mission components, combining culture characteristics, colony and cell morphology, 61-core-gene phylogeny, and comparative functional genomics. Collectively, findings supported proposal of six novel species: *Cladosporium prattiae*, *Cladosporium crawfordii*, *Waltergamsia balasubramanianii*, *Phaeophleospora burdickii*, *Spissiomyces californiae*, and *Neocatenulostroma huberi*. The 61 protein-coding genes generally provided greater species-level resolution than more widely used ITS and LSU. The two *C. crawfordii* isolates - independently recovered from separate facilities - formed a discrete, maximally supported clade distinct from the *C. perangustum* ex-type lineage. The remaining taxa were also resolved as distinct phylogenetic lineages, although interpretation was constrained by locus discordance and the unavailability of whole-genome sequences for ex-type strains. Genome sizes of the examined strains during this study ranged from 25.6 to 62.5 Mb. Genomes varied in predicted gene content, carbohydrate-active enzymes, and biosynthetic gene clusters. Comparative functional genomics revealed predicted stress-response, pigmentation, iron-acquisition pathways consistent with persistence in oligotrophic environments, and traits of potential biotechnological relevance. These findings underscore the importance of fungal surveillance for identifying persistent contaminants, evaluating their survival potential, and strengthening contamination-control strategies across pharmaceutical, medical, and aeronautical industries, as well as planetary protection and microbial control within closed human habitats during future NASA exploration missions.

Keywords: spacecraft assembly cleanrooms; Mars 2020; fungal diversity; novel fungal species; integrative taxonomy; multilocus phylogeny; comparative genomics; planetary protection

INTRODUCTION

Fungi are relatively understudied members of interdependent microbial communities within controlled environments used by pharmaceutical, medical, aeronautical, and space industries (Sandle 2021; Blachowicz et al. 2022). They have been detected in pharmaceutical and clinical environments and spacecraft-assembly facilities, where they may affect product quality, safety, and contamination-control objectives (Kawai et al. 2019; Tršan et al. 2019; Belizario et al. 2021; Blachowicz et al. 2022). Some fungi can withstand stringent monitoring and cleaning protocols likely relying on a combination of melanization and morphological and metabolic plasticity conferring tolerance to desiccation, radiation, oxidative stress, and nutrient limitation (Gostinčar et al. 2012; Casadevall et al. 2017; Dijksterhuis 2019).

Spacecraft-assembly cleanrooms reduce bioburden through HEPA filtration, restricted access, gowning, cleaning, and disinfection, but do not achieve sterility (Benardini et al. 2014). In these settings, low-abundance microbial taxa pose a challenge to environmental sampling and culture-based and culture-independent detection (La Duc et al. 2012). However, fungal species recovered from these oligotrophic environments should not be assumed to have evolved within the cleanroom. Their persistence instead plausibly reflects pre-existing traits that enabled their introduction and consequent survival and detection over competitors that were suppressed. Potential introduction routes include personnel, construction materials, spacecraft components, garments, and equipment (Moissl-Eichinger et al. 2015; Blachowicz et al. 2022).

Several sampling campaigns and complementary cultivation efforts in the Mars 2020 assembly facilities at the JPL Spacecraft Assembly Facility (JPL-SAF) and Kennedy Space Center Payload Hazardous Servicing Facility (KSC-PHSF) recovered 71 fungal isolates across 28 distinct species, including 13 isolates with low similarity to recognized taxa (Blachowicz et al. 2022). Subsequent integration of whole-genome sequencing (WGS), multilocus sequence analysis (MLSA), morphology, and functional assays resolved seven novel species, including two representing novel genera (Parker et al. 2022; Chander et al. 2023; Chander et al. 2024). This study builds on that work by resolving six additional novel species represented by seven isolates recovered in multiple sampling campaigns using a variety of sampling devices, media, and chloramphenicol treatments, indicating that no single sampling and cultivation strategy captured the full novel diversity.

Fungal taxonomy can be complicated by the morphological convergence of taxonomically distant fungal species or within-species phenotypic plasticity, as well as by the presence of incomplete or inaccurate entries in publicly available databases (Lücking et al. 2020). Genomic comparison of broader sets of protein-coding genes and authenticated ex-type material can provide greater taxonomic resolution among closely related species (Taylor et al. 2000; Schoch et al. 2012). Species delimitation can, therefore, be strengthened by integrating culture characteristics, colony and cell morphology, MLSA, and phylogenomics (Taylor et al. 2000; Quaedvlieg et al. 2014). Whole-genome data additionally reveal genes associated with environmental adaptation and biosynthetic gene clusters (BGCs) encoding secondary metabolites (Wisecaver and Rokas 2015; Keller 2019). These functional features can distinguish the ecological and biotechnological potential of novel fungi but should complement, rather than independently determine, taxonomic boundaries.

Current planetary protection monitoring programs primarily target bacterial endospores (Benardini et al. 2014) and consequently overlook fungal bioburden (Blachowicz et al. 2022). However, the previously reported survival in spacecraft-assembly cleanrooms of *Aspergillus* under radiation, neutron exposure, and dry-heat treatments showed that fungi can, also seldom, withstand space-

relevant stresses (Chander et al. 2026). This supports the importance of implementing fungal targets into the current risk-based monitoring programs.

In this study, we characterized seven fungal isolates recovered from Mars 2020 mission assembly cleanrooms and determined their taxonomic status using an integrative framework combining colony and cell morphology, MLSA, and genome-scale phylogeny. We further mined their genome characteristics, predicted functional traits and BGCs to assess possible ecological adaptations and interactions (within the low-abundance microbiome), as well as biotechnological relevance. Collectively, this work aimed to resolve six previously unrecognized species, clarify their relationships to authenticated reference taxa, and expand understanding of the taxonomic and functional diversity of fungi persisting in oligotrophic controlled environments.

MATERIALS AND METHODS

Environmental Sampling and Recovery of Fungal Isolates

The seven fungal isolates examined in this study originated from four environmental sampling campaigns conducted in 2018 at JPL-SAF and KSC-PHSF during assembly of the Mars 2020 mission. The sampling design, collection devices, sample extraction, handling controls, chloramphenicol treatment, and primary cultivation procedures were described in detail previously (Blachowicz et al. 2022). Briefly, BiSKit samplers, flight-certified polyester wipes, and ClipperMops were used according to facility and flight-hardware constraints, and recovered material was concentrated before cultivation on fungal media.

In total, 71 fungal strains isolated from two NASA mission assembly cleanrooms were purified and identified (Blachowicz et al., 2022). The seven isolates representing six novel species, which are taxonomically characterized and described in this study are FJI-L7-BK-DG1, FJII-L10-SW-DR1, FKII-L3-CM-PAB1, FKII-L8-BK-P5, FKII-L3-CM-PAB3, FJII-L1-SW-P2, and FJI-L3-BK-P2.

Morphological Characterization

For colony morphology and microscopic characterization, we followed previously described procedures (Chander et al., 2022). Light-microscopic images were acquired using an Olympus BX53 microscope equipped with a DP25 camera and cellSens software. Differential interference contrast images were obtained using a Nikon Ti2-E inverted microscope and NIS-Elements software. Morphological observations were integrated with molecular phylogenetic evidence for species delineation following an integrative taxonomic approach (Lücking et al. 2020). ITS sequencing and preliminary taxonomic assignment for the isolates were considered as described previously (Blachowicz et al. 2022).

Whole-Genome Sequencing and Assembly

Whole-genome sequencing of the fungal isolates was performed using the workflow described previously (Chander et al. 2023). Briefly, genomic DNA was extracted from approximately 1 g of fungal biomass using the ZymoBIOMICS MagBead DNA kit (Zymo Research, Irvine, CA, USA). Dual-indexed sequencing libraries were prepared using the Nextera DNA Flex workflow (Illumina, San Diego, CA, USA) and sequenced on an Illumina NovaSeq 6000 platform to generate 150-bp paired-end reads. Raw reads were quality-filtered using NGS QC Toolkit v2.3 (Patel and Jain 2012) and assembled *de novo* with SPAdes v3.15.4 (Bankevich et al. 2012). Draft assemblies were subsequently processed using Automatic Assembly for the Fungi (https://github.com/stajichlab/AAFTF) v0.3.3, including contaminant removal, assembly refinement, polishing with Pilon v1.24 (Walker et al. 2014), and scaffold organization. Assembly

156 statistics and overall quality were evaluated using QUAST v5.1.0 (Gurevich et al. 2013). The
157 resulting genome assemblies were deposited in GenBank (Table 1).

158 **Multilocus Phylogenetic Analyses**

159 Species-level phylogenetic relationships were evaluated using multilocus sequence analysis (MLSA)
160 incorporating taxonomically informative fungal markers. Depending on sequence availability and the
161 taxonomic group examined, loci included the nuclear ribosomal internal transcribed spacer (ITS),
162 large-subunit (LSU) and small-subunit (SSU) rRNA regions, translation elongation factor 1-α (*tef1-a*),
163 the second-largest subunit of RNA polymerase II (*rpb2*), actin (*act*), and β-tubulin (*tub2*) (Scholz et al.
164 2012; Stielow et al. 2015).

165 Target loci were recovered from genome assemblies (Supplemental File SF1) using BLASTn
166 (Camacho et al. 2009), and homologous sequences from phylogenetically relevant reference and type
167 strains were retrieved from GenBank. Individual loci were aligned using PASTA (Mirarab et al.
168 2014) and trimmed with ClipKIT v1.3.0 in smart-gap mode to remove gap-rich and phylogenetically
169 uninformative positions (Steenwyk et al. 2020). The trimmed loci were concatenated, and maximum-
170 likelihood phylogenies were reconstructed using IQ-TREE v2.1.1 (Minh et al. 2020). Optimal
171 nucleotide-substitution models were selected with ModelFinder (Kalyaanamoorthy et al. 2017).
172 Nodal support was assessed using 1,000 ultrafast bootstrap replicates and the SH-like approximate
173 likelihood-ratio test (SH-aLRT) (Guindon et al. 2010; Hoang et al. 2017). Phylogenetic placement
174 was interpreted together with morphological characteristics following an integrative taxonomic
175 approach to determine whether the cleanroom isolates represented previously described or novel
176 fungal species (Lücking et al. 2020).

177 ***De Novo* and Functional Genome Annotation**

178 Gene prediction and functional annotation were performed using Funannotate v.1.8.17. Low-
179 complexity soft-masking was initially performed using tantan v51 (Frith 2010). RepeatModeler
180 (Flynn et al. 2020) v2.0.7 was used to generate *de novo* a curated library of repetitive sequences.
181 Genomes were subsequently masked with RepeatMasker v4.2.2 (Tarailo-Graovac and Chen 2009).
182 Gene predictions were generated using BRAKER3 v3.0.8 (Gabriel et al. 2024). Resulting GFF3 files
183 were fed into the "annotate" function from Funannotate v1.8.17 for functional annotation
184 integrated with eggNOG-mapper v2.1.13 (database v5.0.2) and fungiSMASH, the fungal
185 implementation of antiSMASH v8 (Blin et al. 2025). BUSCO v6.0.0 (Tegenfeldt et al. 2024) was
186 used to assess lineage-specific completeness of genomes and functional annotations.

187 **Whole Genome-Based Phylogenomic Analysis**

188 A genome-scale phylogenomic analysis was performed using UFCG v1.0.6 (Kim et al. 2022). In
189 total, 81 whole-genome assemblies representing 81 Ascomycota species were obtained from the
190 NCBI GenBank reference genome database. The species were selected to represent the taxonomic
191 vicinity of the novel isolates, together with representatives of two ingroup genera (*Aureobasidium* and
192 *Trichoderma*) and two outgroup taxa (Saccharomycotina and Pezizomycetes) to anchor their
193 phylogenetic placement. The full list of genomes used in this analysis is provided in (Supplemental
194 Table ST1).

195 Profiles of 61 core gene markers (Kim et al. 2022) were extracted from the 81 genome assemblies
196 and seven isolates using the UFCG profile module. A phylogenetic tree was then reconstructed from
197 these profiles using the UFCG tree module. Specifically, the extracted markers were aligned using
198 MAFFT L-INS-i v7.525 (Katoh and Standley 2013), and alignment columns containing more than
199 50% gaps were removed. A maximum-likelihood tree was inferred from the concatenated

alignments using IQ-TREE v3.0.1 (Wong et al. 2026) under the LG+I+G4 evolutionary model, with branch support assessed using 1,000 ultrafast bootstrap replicates. The resulting tree was visualized using FigTree v1.4.4.

RESULTS & DISCUSSION:

Differential Recovery of Novel Fungal Species

Recovery varied by facility and sampling campaign. The first JPL-SAF campaign yielded *Neocatenulostroma huberi* FJI-L3-BK-P2 and *Cladosporium prattiae* FJI-L7-BK-DG1, whereas the second yielded *Spissiomyces californiae* FJII-L1-SW-P2 and *C. crawfordii* FJII-L10-SW-DR1. No novel species were recovered during the first KSC-PHSF campaign; the second yielded *C. crawfordii* FKII-L3-CM-PAB1, *Phaeophleospora burdickii* FKII-L3-CM-PAB3, and *Waltergamsia balasubramanianii* FKII-L8-BK-P5. The independent recovery of *C. crawfordii* during the second campaigns at both JPL-SAF and KSC-PHSF indicated that this species was not restricted to a single facility.

Cultivation media and sampling methods provided complementary recovery profiles. Five strains, each representing a novel species—*N. huberi*, *S. californiae*, *W. balasubramanianii*, *C. crawfordii*, and *P. burdickii*—were isolated on potato dextrose agar (PDA). *Cladosporium prattiae* was isolated on dichloran glycerol (DG) agar, whereas a second strain of *C. crawfordii* was isolated on dichloran rose bengal chloramphenicol (DRBC) agar. Chloramphenicol treatment preceded the recovery of *C. crawfordii* FKII-L3-CM-PAB1 and *P. burdickii* FKII-L3-CM-PAB3; the other five strains were recovered without antibiotic treatment. BiSKit sampling recovered *N. huberi*, *W. balasubramanianii*, and *C. prattiae*; ClipperMop sampling recovered *C. crawfordii* FKII-L3-CM-PAB1 and *P. burdickii*; and polyester-wipe sampling recovered *S. californiae* and *C. crawfordii* FJII-L10-SW-DR1.

Overall, six novel fungal species represented by seven isolates were recovered through complementary sampling and cultivation approaches, showing that the cultivable fungal diversity detected in these low-biomass cleanroom environments depended on sampling location and time, collection device, growth medium, and antibiotic treatment. Where available, authenticated ex-type strains were used to evaluate species-delimitation hypotheses, with concordance between MLST and 61 conserved core-gene phylogenies providing additional support for species recognition and phylogenetic placement (Taylor et al. 2000; Schoch et al. 2012; Quaedvlieg et al. 2014).

Taxonomic Characteristics of Novel Species

Cladosporium prattiae Venkatesw., A.M. Chander & Nitin K. Singh, sp. nov.

MycoBank: MB 844471

Etymology: prattiae (pratt'i.ae; N.L. gen. n. prattiae, of Pratt), named in honor of Prof. Lisa A. Pratt, former NASA Planetary Protection Officer, in recognition of her contributions to planetary protection, astrobiology, and the understanding of life in extreme environments.

1. Diagnosis

Cladosporium prattiae was distinguished from *C. austrohemisphaericum* and other members of the *C. sphaerospermum* species complex by differences in ITS and *act*, its independent position in the concatenated ITS–*tef1*–*act* phylogeny, and its cultural and microscopic characteristics. Among the loci examined, *act* and *tef1* provided the strongest species-level discrimination.

2. Description

Colonies on PDA are approximately 29 mm in diameter after 14 d incubation at room temperature, olive-green to brown, and circular (Fig. 1-1A). Colonies on PDA appear with conspicuous radially

extending ridges and furrows originating from the colony center. Vegetative hyphae are smooth-walled, septate, erect, and sparingly branched. Conidiophores are erect, arising from vegetative hyphae, simple to sparingly branched. Conidia are produced in chains, predominantly sub-globose, ovoid to ellipsoidal, with a mean size of 3.19 × 2.28 μm (n = 10) (Fig. 1-1B and 1-1C). No single stable microscopic character unequivocally separates it from *C. austrohemisphaericum*.

3. Holotype and Ecology/Distribution

Holotype: isolated on 17 April, 2018 by K. Venkateswaran at the Jet Propulsion Laboratory Spacecraft Assembly Facility (JPL-SAF) Pasadena, California, USA (34.1478° N, 118.1445° W) from the cleanroom floor, where Mars 2020 mission components were assembled. Holotype - NRRL B-64423 - is permanently preserved in a metabolically inactive state. Isotype culture: DSM 114620 is cryopreserved in a metabolically inactive state.

Ecology and distribution: known only from the type locality.

4. Molecular and Phylogenetic Characterization

C. prattiae FJI-L7-BK-DG1 was distinguished from *C. austrohemisphaericum* CBS 140482 by pairwise comparisons of ITS [498/503 identities (99%); five nucleotide substitutions], *tef1* [871/914 identities (95%); 43 nucleotide substitutions], and *act* [214/224 identities (95.54%); nine nucleotide substitutions and one gap] (Table 1; Supplemental Alignment File SAF-1). In the concatenated ITS–*tef1*–*act* phylogeny, the isolate formed an independent branch within the *C. sphaerospermum* species complex rather than clustering with CBS 140482 or DTO 305-E8; the node linking it with COAD 3487 and COAD 3351 received 72.1% support (Fig. 2). The differentiation observed in *act*, together with the multilocus placement, supported recognition of *C. prattiae* and was consistent with the established value of *act* and *tef1-a* for resolving *Cladosporium* species (Bensch et al. 2012; Tan et al. 2024). At the genome scale, phylogenetic analysis based on 61 conserved core markers resolved the focal isolate as a distinct lineage within Cladosporiaceae (Fig. 3), providing additional support for its phylogenetic placement. Collectively, the sequence differences, multilocus and genome-scale phylogenetic evidence, and cultural and microscopic characteristics supported recognition of *C. prattiae* as a novel species.

5. Genome Characteristics

The draft genome of FJI-L7-BK-DG1 is deposited in NCBI under WGS accession JAKLLY000000000. The assembly (N50 = 1.16 Mb; L50 = 10) comprises 72 scaffolds totaling 29.4 Mb and has 4.64% repetitive DNA and 53.22% GC content. The draft genome counts 11,140 predicted genes; 11,932 mRNAs; 10,776 EggNOG, 8,595 Pfam, 546 CAZyme annotations (Table 2).

***Cladosporium crawfordii* Venkatesw., A.M. Chander & Nitin K. Singh, sp. nov.**

MycoBank: MB 844483

Etymology: crawfordii (craw'ford.i.i; N.L. gen. n. crawfordii, of Crawford), named posthumously in honor of the late Prof. Ronald L. Crawford, University of Idaho, in recognition of his contributions to microbiology and the molecular biology of microorganisms from extreme environments.

1. Diagnosis

C. crawfordii was distinguished from *C. perangustum* and related members of the *C. perangustum* species complex by differences in *act* and *tef1*, its distinct placement in the concatenated ITS–*tef1*–*act* phylogeny, and its cultural and microscopic characteristics. ITS alone did not distinguish the species,

whereas the protein-coding loci provided species-level resolution. The conspecific placement of the two geographically separated isolates was also supported by the 61-core-gene phylogeny.

2. Description

Colonies on PDA are circular, brown to olivaceous-brown, with a paler peripheral margin and conspicuous radial furrows extending outward from the central region (Fig. 1-2A); reverse is dark gray-brown to olivaceous. Vegetative hyphae are septate, smooth to apparently smooth-walled, relatively slender and branching. Conidiophores are erect, arising from vegetative hyphae, mostly simple or sparsely branched (Fig. 1-2B). Conidiogenous structures are terminal, bearing small clustered or short-chain conidia. Conidia are predominantly ovoid to ellipsoidal or sub-globose (Fig. 1-2C).

3. Holotype and Ecology/Distribution

Holotype: isolated on 25 September, 2018 by K. Venkateswaran from the JPL-SAF cleanroom floor, (Pasadena, California, USA; 34.1478° N, 118.1445° W), where Mars 2020 mission components were assembled. Holotype - NRRL B-64425 - is permanently preserved in a metabolically inactive state. Isotype culture: DSM 114728 is cryopreserved in a metabolically inactive state.

Additional material examined: KSC-PHSF cleanroom floor sample (Cape Canaveral, Florida, USA).

Ecology and distribution: Two isolates of *Cladosporium crawfordii* (FJII-L10-SW-DR1 and FKII-L3-CM-PAB1) were independently recovered from geographically separated facilities, the JPL-SAF in California and KSC-PHSF in Florida.

4. Molecular and Phylogenetic Characterization

Analysis of ITS, *tef1-a*, and *act* resolved isolates previously identified as *C. perangustum* into five groups. FJII-L10-SW-DR1 and FKII-L3-CM-PAB1 were placed in Group I, which received maximal support (100% maximum-likelihood bootstrap/1.0 Bayesian posterior probability/100% maximum-parsimony bootstrap) and was distinct from the lineage containing the *C. perangustum* ex-type strain CBS 125996 (93%/1.0/84%; Fig. 4; Supplemental Table ST2). Relative to CBS 125996, the focal isolate showed 100% ITS, 91.19% *tef1-a*, and 97.79% *act* identity; the corresponding ranges among Group I isolates were 99.81–100%, 87.45–92.66%, and 94.25–98.23%, respectively (Table 1; Supplemental Alignment File SAF-2). Pairwise alignments independently confirmed complete ITS identity [516/516 identities (100%)] and differentiation at *act* [221/226 identities (97.79%); five nucleotide substitutions] between FKII-L3-CM-PAB1 and CBS 125996. Thus, *tef1-a* and *act* provided greater species-level resolution than ITS alone, consistent with established multilocus practice in *Cladosporium* (Bensch et al. 2012). At the genome scale, phylogenetic analysis based on 61 conserved core markers resolved the two focal isolates as a discrete clade within Cladosporiaceae with 100% support (Fig. 3), providing additional evidence that they represented a single genomic lineage. Collectively, the protein-coding-locus differentiation and concordant multilocus and genome-scale phylogenetic evidence supported recognition of this lineage as *C. crawfordii*.

5. Genome Characteristics

The draft genome of FJII-L10-SW-DR1 is deposited in NCBI under WGS accession JAKLMJ000000000. The assembly (N50 = 1.30 Mb; L50 = 9) comprises 155 scaffolds totaling 31.0 Mb and has 6.78% repetitive DNA and 52.40% GC content (Table 2). The draft genome counts 11,403 predicted genes; 12,208 mRNAs; 11,107 EggNOG, 8,921 Pfam, 563 CAZyme annotations.

The draft genome of FKII-L3-CM-PAB1 is deposited in NCBI under WGS accession JAKLNF000000000. The assembly (N50 = 1.79 Mb; L50 = 8) comprises 195 scaffolds totaling 31.7

Mb and has 6.70% repetitive DNA and 52.30% GC content (Table 2). The draft genome counts 11,560 predicted genes; 12,385 mRNAs; 11,237 EggNOG, 9,009 Pfam, 561 CAZyme annotations.

***Waltergamsia balasubramanianii* Venkatesw., A.M. Chander & Nitin K. Singh, sp. nov.**

MycoBank: MB 844480

Etymology: balasubramanianii (ba.la.su.bra.ma'ni.i.i; N.L. gen. n. balasubramanianii, of Balasubramanian), named posthumously in honor of the late Prof. K. Balasubramanian for his contributions to marine biology.

1. Diagnosis

Waltergamsia balasubramanianii was distinguished from currently recognized *Waltergamsia* species by differences in ITS, LSU, *rpb2*, and *tef1*, its independent position in the concatenated multilocus phylogeny, and its cultural and microscopic characteristics. The combined evidence supported its recognition as a distinct hypocrealean species.

2. Description

Colonies on PDA are broadly circular, cream-white to pale gray-white on the obverse. A dense, finely textured aerial mycelium and occasional radial folding or furrowing are observed toward the center (Fig. 1-3A). Reverse is tan to ochre or pale orange-brown, darker centrally. Vegetative hyphae are hyaline, smooth-walled to apparently smooth-walled, septate, and branched. Conidiogenous structures are simple, slender, and erect, occasionally branched. Conidia are terminal in compact heads or clusters, predominantly sub-globose, ovoid to short ellipsoidal, and hyaline (Fig. 1-3B and 1-3C).

3. Holotype and Ecology/Distribution

Holotype: isolated on 24 July, 2018 by K. Venkateswaran from the KSC-PHSF cleanroom floor (Cape Canaveral, Florida, USA; 28° 23' 48.6" N, 80° 36' 20.4" W), where Mars 2020 mission components were assembled. Holotype - NRRL 64428 - is permanently preserved in a metabolically inactive state. Isotype culture: DSM 114627 is cryopreserved in a metabolically inactive state.

Ecology and distribution: known only from the type locality.

4. Molecular and Phylogenetic Characterization

W. balasubramanianii FKII-L8-BK-P5 differed from *W. citrina* CBS 384.96 in ITS [497/524 identities (95%); 22 nucleotide substitutions and five gaps], from *W. hennebertii* CBS 768.69 in LSU [833/844 identities (99%); nine nucleotide substitutions and two gaps], and from *W. alkalina* CBS 741.94 in *rpb2* [707/755 identities (94%); 48 nucleotide substitutions] and *tef1* [803/811 identities (99%); eight nucleotide substitutions] (Table 1; Supplemental Alignment File SAF-3). In the concatenated phylogeny, the isolate formed an independent branch within a lineage containing AF502849.1, AF502848.1, and NZD-mf165 (86/68 support) and was separated from *W. citrina* CBS 384.96, *W. hennebertii* CBS 768.69, and *W. fusidioides* CBS 840.68 (Fig. 5). Genome-scale phylogenetic analysis based on 61 conserved core markers supported the placement of the strain within Hypocreales (Sordariomycetes) and provided additional evidence for its recognition as a distinct lineage (Fig. 3). The strain was assigned to *Waltergamsia* following the phylogenetic revision in which *Acremonium citrinum*, *A. hennebertii*, and *A. fusidioides* were transferred to this genus (Hou et al. 2023). The observed sequence divergence, independent multilocus placement, and diagnostic cultural and microscopic characteristics collectively supported recognition of *W. balasubramanianii* as a novel species.

5. Genome Characteristics

The draft genome of FKII-L8-BK-P5 is deposited in NCBI under WGS accession JAKLNE000000000. The assembly (N50 = 479,776 bp; L50 = 24) comprises 86 scaffolds totaling 34.5 Mb, and has 1.51% repetitive DNA and 50.00% GC content. The draft genome counts 11,053 predicted genes; 11,662 mRNAs; 11,175 EggNOG, 9,119 Pfam, 490 CAZyme annotations (Table 2).

***Phaeophleospora burdickii* Venkatesw., A.M. Chander & Nitin K. Singh, sp. nov.**

MycoBank: MB 844484

Etymology: burdickii (bur'dick.i.i; N.L. gen. n. burdickii, of Burdick), named in honor of Gary Burdick, former Program Manager at JPL, for contributions to the management and implementation of NASA space missions.

1. Diagnosis

Phaeophleospora burdickii was distinguished from currently recognized *Phaeophleospora* species by pronounced divergence at *tef1*, its independent position in the concatenated ITS–LSU–*tef1* phylogeny, and its cultural and microscopic characteristics. ITS and LSU alone provided insufficient species-level resolution, whereas *tef1* supplied the principal molecular evidence for delimitation.

2. Description

Colonies on oatmeal agar are circular to broadly circular, pale tan, salmon-brown to orange-brown, darker centrally, with concentric growth zones (Fig. 1-4A). Reverse is orange-brown to reddish-brown and more intensely pigmented centrally. Vegetative hyphae are branched, septate, smooth to apparently smooth-walled. Conidiogenous structures are simple to branched (Fig. 1-4B). Conidia are numerous, predominantly ellipsoidal to cylindrical or somewhat fusiform, with rounded ends; some elongated structures appear transversely septate (Fig. 1-4C).

3. Holotype and Ecology/Distribution

Holotype: isolated 24 July, 2018 by K. Venkateswaran from the KSC-PHSF cleanroom floor (Cape Canaveral, Florida, USA; 28° 23' 48.6" N, 80° 36' 20.4" W), where Mars 2020 mission components were assembled. Holotype - NRRL 64430 m- is permanently preserved in a metabolically inactive state. Isotype culture: DSM 114629 is cryopreserved in a metabolically inactive state.

Ecology and distribution: known only from the type locality.

4. Molecular and Phylogenetic Characterization

P. burdickii FKII-L3-CM-PAB3 differed from *P. eucalypticola* CPC 26523 in ITS [562/565 identities (99%); three gaps], LSU [891/892 identities (99%); one nucleotide substitution], and *tef1* [471/513 identities (92%); 34 nucleotide substitutions and eight gaps] (Table 1; Supplemental Alignment File SAF-4). The isolate formed a distinct branch in the concatenated ITS–LSU–*tef1* phylogeny, with 78.7/74 support at the relevant ancestral node (Fig. 6). Although ITS and LSU provided limited species-level resolution, the pronounced *tef1* divergence and independent multilocus placement supported recognition of *P. burdickii* as a distinct species under a genealogical concordance approach (Taylor et al. 2000). Phylogenetic analysis based on 61 conserved core markers further placed the strain within Dothideomycetes, near the Mycosphaerellaceae-associated radiation (Fig. 3). Because no *Phaeophleospora* reference genome was available for inclusion in the core-marker phylogeny, the genus- and species-level interpretation was based primarily on the taxonomically focused concatenated phylogeny, protein-coding-locus divergence, and cultural and microscopic characteristics.

5. Genome Characteristics

The draft genome of FKII-L3-CM-PAB3 is deposited in NCBI under WGS accession JAKLNG000000000. The assembly (N50 = 1.62 Mb; L50 = 7) comprises 55 scaffolds totaling 31.6 Mb, and has 1.28% repetitive DNA and 53.14% GC content. The draft genome counts 12,600 predicted genes; 15,848 mRNAs; 13,926 EggNOG, 10,629 Pfam, 629 CAZyme annotations (Table 2).

***Spissiomyces californiae* Venkatesw., A.M. Chander & Nitin K. Singh, sp. nov.**

MycoBank: MB 844472

Etymology: californiae (ca.li.for'ni.ae; N.L. gen. n. californiae, of California), named after California, USA, the geographic origin of the type strain.

1. Diagnosis

Spissiomyces californiae was distinguished from currently recognized *Spissiomyces* and related *Neospissiomyces* species by differences in ITS, LSU, SSU, *rpb2*, and particularly *tub2*, together with its independent position in the concatenated multilocus phylogeny and its distinctive dark, compact culture morphology. Among the loci examined, *tub2* provided the strongest species-level discrimination.

2. Description

Colonies on PDA are dark brown to black, compact, irregularly circular to lobate, markedly raised and rugose, with pronounced folding (Fig. 1-5A); reverse is dark gray-brown to black. Vegetative hyphae are pigmented to pale brown, septate, smooth to finely textured, irregularly branched and in places composed of swollen, broadly ovoid to sub-globose cells. Hyphal elements may occur in short chains (Fig. 1-5B). Conidiophore-like structures are simple to sparsely branched. Enlarged spherical, sub-globose or ovoid propagule-like cells are terminal and intercalary; some appear thick-walled and multicelled or septate (Fig. 1-5C).

3. Holotype and Ecology/Distribution

Holotype: isolated 25 September, 2018 by K. Venkateswaran from the JPL-SAF cleanroom floor (Pasadena, California, USA; 34.1478° N, 118.1445° W), where Mars 2020 mission components were assembled. Holotype - NRRL 64432 – is permanently preserved in a metabolically inactive state. Isotype culture: DSM 114631 is cryopreserved in a metabolically inactive state.

Ecology and distribution: known only from the type locality.

4. Molecular and Phylogenetic Characterization

S. californiae FJII-L1-SW-P2 differed from *Neospissiomyces floridanus* CPC 45908 in ITS [553/558 identities (99%); five nucleotide substitutions], LSU [446/447 identities (99%); one nucleotide substitution], and *rpb2* [509/516 identities (99%); seven nucleotide substitutions], and from *Spissiomyces ramosus* CGMCC 3.17076 in SSU [1019/1020 identities (99%); one nucleotide substitution] and *tub2* [751/829 identities (91%); 69 nucleotide substitutions and nine gaps] (Table 1; Supplemental Alignment File SAF-5). In the concatenated phylogeny, the isolate formed a distinct branch within a maximally supported clade containing related *Spissiomyces* and *Neospissiomyces* taxa. The substantial *tub2* divergence, distinct multilocus placement, and characteristic dark, compact culture morphology supported recognition of *S. californiae* as a novel species. In the MLSA phylogeny, the isolate formed a distinct branch sister to the *Spissiomyces aggregatus* type strain CGMCC 3.17072 (89.1/98), and this pair was sister to the *S. ramosus* type strain CGMCC 3.17077 within a

maximally supported clade (100/100) (Fig. 7). Genome-scale phylogeny based on 61 conserved core markers placed the strain within Dothideomycetes near Aplosporella/Botryosphaeriales references. Due to inadequate *Spissiomyces* representation in the dataset, genus- and species-level delineation relied primarily on the focused MLSA and phenotype (Crous et al. 2004) (Fig. 3).

5. Genome Characteristics

The draft genome of FJII-L1-SW-P2 is deposited in NCBI under WGS accession JAKLMF000000000. The assembly ((N50 = 14,013 bp; L50 = 530) comprises 3,910 scaffolds totaling 25.6 Mb, and has 2.23% repetitive DNA and 53.72% GC content. The draft genome counts 9,120 predicted genes; 9,767 mRNAs; 9,068 EggNOG, 6,840 Pfam, 308 CAZyme annotations. The current assembly is highly fragmented, a limitation which should be accounted for during comparative analysis (Table 2).

***Neocatenulostroma huberi* Venkatesw., A.M. Chander & Nitin K. Singh, sp. nov.**

MycoBank: MB 844482

Etymology: huberi (hu'ber.i.i; N.L. gen. n. huberi, of Huber), named in honor of Prof. Harald Huber, University of Regensburg, for contributions to the microbiology of extremophiles.

1. Diagnosis

N. huberi was distinguished from currently recognized *Neocatenulostroma* species by differences in ITS and the protein-coding loci *rpb2*, *tub2*, and *tef1*, together with its independent position in the concatenated multilocus phylogeny and its cultural and microscopic characteristics. LSU alone did not provide species-level resolution, whereas *rpb2* and *tub2* provided the strongest molecular discrimination. Collectively, the molecular, phylogenetic, and morphological evidence supported recognition of *N. huberi* as a novel species.

2. Description

Colonies on PDA agar are compact, circular to broadly circular, darkly pigmented, with a yellow-olive to brown surface, and darker center (Fig.1-6A). The reverse is dark olive-brown to nearly black. Vegetative hyphae are pigmented, smooth to finely textured, septate and branched. Cells are cylindrical, rectangular, broadly ellipsoidal, or swollen-subglobose. Some hyphae form short chains of thick-walled pigmented cells (Fig. 1-6B). Propagule-bearing structures are terminal or lateral; propagule-like cells are ovoid, ellipsoidal to sub-globose, sometimes transversely septate, singly or in short chains (Fig. 1-6C).

3. Holotype and Ecology/Distribution

Holotype: isolated 17 April, 2018 by K. Venkateswaran from the JPL-SAF cleanroom floor (Pasadena, California, USA; 34.1478° N, 118.1445° W), where Mars 2020 mission components were assembled. Holotype - NRRL B-64422 – is permanently preserved in a metabolically inactive state. Isotype culture: DSM 114619 is cryopreserved in a metabolically inactive state.

Ecology and distribution: known only from the type locality.

4. Molecular and Phylogenetic Characterization

N. huberi FJI-L3-BK-P2 differed from *N. germanicum* CBS 539.88 in ITS [521/526 identities (99%); three nucleotide substitutions and two gaps], although their LSU sequences were identical [891/891 identities (100%)]. It also differed from *N. spinulosum* FMR 18793 in *rpb2* [813/854 identities (95%); 41 nucleotide substitutions] and *tef1* [786/806 identities (98%); 20 nucleotide substitutions], and

from *N. microsporum* CBS 101951 in *tub2* [234/255 identities (92%); 20 nucleotide substitutions and one gap] (Table 1; Supplemental Alignment File SAF-6). In the concatenated phylogeny, the isolate formed an independent lineage distinct from the type-derived lineages of *N. germanicum*, *N. microsporum*, *N. abietis*, and *N. pinorum*. The pronounced divergence in *rpb2* and *tub2*, together with its multilocus placement and distinctive cultural and microscopic characteristics, supported recognition of *N. huberi* as a novel species (Fig. 8). Its separate phylogenetic placement, together with divergence at the protein-coding loci, supports recognition as *N. huberi*, consistent with the multilocus framework used to delimit *Neocatenulostroma* and related Teratosphaeriaceae (Quaedvlieg et al. 2014). In the genome-scale phylogeny based on 61 conserved core markers, the isolate clustered within the Teratosphaeriaceae clade. As no authenticated *Neocatenulostroma* reference genome was available for comparison, genus- and species-level delineation relied on the focused MLSA, locus divergence, and phenotype (Fig. 3).

5. Genome Characteristics

The draft genome of FJI-L3-BK-P2 is deposited in NCBI under WGS accession JAKLLW000000000. The assembly (N50 = 24,718 bp; L50 = 733) comprises 4,993 scaffolds totaling 62.5 Mb, and has 1.40% repetitive DNA and 54.24% GC content. The draft genome counts 27,880 predicted genes; 28,876 mRNAs; 24,051 EggNOG annotations; 16,685 Pfam assignments; 791 CAZymes (Table 2). The current assembly is highly fragmented, a limitation which should be accounted for during comparative analysis.

The assembled genome size is approximately twice that reported for many haploid Teratosphaeriaceae genomes, suggesting the presence of a diploid genomic complement. Consistently, BUSCO analysis estimated >99% completeness, <1% contamination, but >95% duplication, in line with extensive genome-wide duplication. Moreover, 99.72% of the sequencing reads mapped back to the assembly, indicating that the duplicated sequences are well represented in the sequencing dataset rather than arising predominantly from unsupported or contaminant contigs. A mean sequencing depth of 51× further supports the robustness of the assembly and its duplicated sequence complement. Collectively, these observations represent strong evidence for genome-wide duplication and are consistent with a diploid (2n) genome, although alternative explanations, including the separate assembly of highly divergent haplotypes, cannot be excluded without additional ploidy analyses. Because this represents the first WGS available for the genus, reference-dependent approaches requiring a closely related genome may currently have limited utility for resolving ploidy.

Genome-Based Functional Characteristics, Biosynthetic Potential, and Relevance to Future Space Exploration

An overview of the functional characteristics of the seven isolates described in this study is presented in Fig. 9 and Supplementary Table ST3. Detailed results of the COG, BGC, and Pfam analyses are provided in Supplementary Tables ST4, ST5, and ST6, respectively.

It was hypothesized that persistence of the six novel fungal species (seven strains) could be enabled by different combinations of functions related to nutrient acquisition, metabolic flexibility, cellular maintenance, environmental sensing, transport, and secondary metabolism. Accordingly, taxa occupying similarly restrictive environments were not expected to have shared genomic signatures, but rather to achieve similar ecological outcomes through different genomic repertoires. Hypotheses were evaluated by comparing genome size, predicted gene content, carbohydrate-active enzymes (CAZymes), COG-classified markers, Pfam-annotated domains, and BGCs across the seven isolates.

The observed differences, together with the presence of functions relevant to growth and maintenance under resource-limited conditions, were consistent with the proposed model.

Spacecraft assembly facilities are an adequate setting for evaluating this model, due to a combination of low nutrient availability, stringent cleaning regimens, low microbial biomass, controlled humidity and temperature, and prolonged residence on manufactured surfaces. Earlier work showed that viable microorganisms, including fungi, can persist and still be recovered despite repeated cleaning (La Duc et al. 2012; Blachowicz et al. 2022). Although such findings cannot be extrapolated directly to the novel taxa described here, they demonstrate that spacecraft-associated fungi can possess physiologies relevant to survival beyond the cleanroom environment and support further experimental assessment of the candidate functional traits identified in their genomes. Mechanistic validation under specific cleanroom, spacecraft, or Mars-relevant conditions is beyond the taxonomic and comparative genomic scope of the present study.

Overview of Predicted Metabolic Repertoires as Candidate Mechanisms of Persistence

The first hypothesis is that genomes contain complementary systems for maintaining nutrient flux and cellular integrity under oligotrophic stress. *C. prattiae* FJI-L7-BK-DG1 met this expectation, with 11,140 predicted genes, 546 CAZymes, 9627 COG-classified markers. Carbohydrate transport and metabolism, post-translational modification/protein turnover/chaperones, and amino-acid transport and metabolism were the most populated COG categories. These findings are consistent with earlier studies of *Cladosporium*, which have identified broad carbohydrate-utilization capacities associated with growth across adverse environmental conditions (Yew et al. 2016; Ma et al. 2018). Approximately 28% of COG-classified markers in FJI-L7-BK-DG1 were assigned to unknown functions, leaving a substantial fraction of this candidate persistence repertoire unresolved.

The two independently recovered *C. crawfordii* strains allowed assessment of whether genomic features potentially associated with persistence were conserved across isolates from distinct facilities. FJII-L10-SW-DR1 and FKII-L3-CM-PAB1, recovered from JPL-SAF and KSC-PHSF, respectively, had quantitatively similar functional profiles (e.g., 543 vs. 561 CAZymes; 9,989 vs. 10,080 COGs; 31 vs. 33 BGCs), as well as similar BGC profiles. In both genomes, approximately 29% of the COG-classified functions were unknown, whereas carbohydrate metabolism, protein turnover/chaperones, and amino-acid metabolism were among the dominant characterized categories. This concordance suggested that potentially relevant genomic traits were conserved in both settings.

The draft genome of *W. balasubramanianii* FKII-L8-BK-P5 encoded 53 BGCs, the largest BGC repertoire among the novel fungi analyzed here. Carbohydrate metabolism, protein turnover/chaperones, amino-acid metabolism, and secondary-metabolite biosynthesis, transport, and catabolism were the most represented COG categories. The genome of FKII-L8-BK-P5 was comparable in size to the 35.8-Mb genome reported for the phylogenetically neighboring *Acremonium* (*Sarocladium*) *strictum* AAJ6 (34.5 vs. 35.8 Mb; 11,053 vs. 12,568 genes; 490 vs. 775 CAZymes) (Lopes et al. 2020). Production of structurally diverse secondary metabolites in *Acremonium* (now *Waltergamsia*) was previously demonstrated, with over 600 compounds documented across the species of *Acremonium* (Qin et al. 2024). The 53 predicted BGCs identified in FKII-L8-BK-P5 strain also exceed the 42 reported for *A. chrysogenum* (*Hapsidospora chrysogena*) (Terfehr et al. 2014).

P. burdickii FKII-L3-CM-PAB3 also encoded a functional repertoire potentially relevant to limited resource acquisition, growth, and maintenance. Approximately 30% of its 11,884 COG annotations were assigned to unknown functions, whereas among characterized functions, carbohydrate transport and metabolism, secondary-metabolite biosynthesis/transport/catabolism, and protein turnover/chaperones were the most populated categories. The current unavailability of publicly

582 available whole-genome assemblies for *Phaeophleospora* limits direct genomic comparison and suggests
583 the role of this new genome as a resource for an understudied lineage.

584 Whether a smaller biosynthetic repertoire necessarily corresponded to a narrower functional capacity
585 was examined using *S. californiae* FJII-L1-SW-P2. Although this isolate contained the fewest
586 predicted BGCs (n = 10) among the seven isolates, 8,514 COG markers were identified, with broad
587 representation of functions associated with posttranslational modification, protein turnover and
588 chaperones, as well as intracellular trafficking, secretion, and vesicular transport. These systems are
589 central to fungal cellular homeostasis, polar growth, secretion and nutrient cycling and may therefore
590 contribute to responses to changing environmental conditions (Shoji et al. 2014; Pope and Prade
591 2026). This functional profile is consistent with the hypothesis that robust cellular maintenance and
592 trafficking systems may support persistence despite a comparatively small BGC repertoire.

593 The draft genome of *N. huberi* FJI-L3-BK-P2 was likely diploid and an extensive predicted
594 functional repertoire comprising 27,880 genes, 16,685 Pfam-annotated domains, 791 CAZymes, and
595 38 BGCs. Amino-acid transport and metabolism, lipid transport and metabolism, translation,
596 ribosomal structure and biogenesis, and signal-transduction mechanisms were major functional
597 categories. Signal-transduction systems are central to fungal perception of and response to
598 environmental variables, including nutrient availability, osmotic and oxidative stress, pH,
599 temperature, and oxygen availability (Bahn et al. 2007). Accordingly, the combination of a relatively
600 large gene repertoire and representation of metabolic and signal-transduction functions in FJI-L3-
601 BK-P2 isolate is compatible with broad metabolic flexibility and environmental responsiveness.
602 However, because closely related, high-quality whole-genome assemblies were unavailable for direct
603 comparison, it remains unclear whether these genomic features were lineage-specific or reflected
604 biases in assembly and annotation. Additionally, mechanisms involved in protein homeostasis can
605 contribute to signaling during environmental stress (Leach et al. 2012; Roy and Tamuli 2022).
606 Therefore, the repeatedly observed prevalence of functions associated with posttranslational
607 modification, protein turnover, and chaperones is particularly relevant.

608 **Pigmentation Pathways as Candidate Mechanisms of UV and Stress Tolerance**

609 Fungal melanin and related pigments have been associated with protection from UV radiation,
610 oxidative stress, and desiccation (Zhang et al. 2017). It was, therefore, also hypothesized that
611 pigmentation, including melanin-associated genomic traits, potentially contributed to protection
612 from UV radiation and related physicochemical stress. To evaluate this possibility, predicted BGCs
613 were compared with previously characterized clusters linked to experimentally described pigment
614 production and stress-related phenotypes.

615 *C. prattiae* encoded a BGC for a melanin precursor, scytalone, including homologs of PfmaG and
616 PfmaE. In the experimentally characterized reference pathway, *pfmaE* deletion affected conidial
617 development and adherence (Zhang et al., 2017). Similar scytalone-associated BGCs were identified
618 in both *C. crawfordii* strains and in *P. burdickii*. *S. californiae* encoded a protein homolog of the conidial-
619 yellow-pigment polyketide synthase Alb1, required in melanin biosynthesis as previously reported
620 (Oh et al. 2008). Three of the seven isolates described in this study, *C. prattiae* FJI-L7-BK-DG1^T, *S.*
621 *californiae* FJII-L1-SW-P2^T, and *N. huberi* FJI-L3-BK-P2^T, were experimentally shown to be resistant
622 to a UV-C dose of 1,000 J/m² (Blachowicz et al. 2022). However, no melanin-associated traits were
623 predicted in *N. huberi*, while similar scytalone-associated pathways were detected in UV-C-sensitive
624 *C. crawfordii* and *P. burdickii*. Thus, BGC presence alone does not explain UV resistance, which may
625 depend on a more complex pigment production and regulatory network.

626 **Siderophore-Mediated Iron Acquisition under Nutrient Limitation**

Metachelins can be secreted under iron-depleted conditions to support scavenging and transport of environmental iron (Krasnoff et al. 2014). On dry, frequently cleaned manufactured surfaces, iron and other micronutrients may be poorly accessible. Therefore, it was additionally hypothesized that the presence of high-affinity iron-chelating siderophores could have supported fungal persistence under nutrient-limited conditions. *W. balasubramanianii* and *P. burdickii* contained homologs of coprogen/dimerumic-acid siderophore BGCs which were experimentally shown to chelate environmental iron under iron-limited conditions (Zhang et al. 2021).

Although functionality of the predicted siderophore clusters was not demonstrated, their presence suggests enhanced iron acquisition capacity and a competitive advantage in nutrient-poor conditions. Similar iron-acquisition strategies could be relevant to future crewed habitats and associated nutrient-limited built-environment niches. If validated, siderophores can have potential biotechnological applications in metal recovery, bioremediation, and biosensing.

BGC Diversity as a Basis for Chemical Interaction and Biotechnology

Finally, it was hypothesized that beyond its biotechnological potential, BGC diversity might have contributed to chemical competition, signaling, or stress protection. With the largest predicted BGC repertoire, *W. balasubramanianii* encoded predicted homologs of the fusaridione A and fusaristatin A BGCs. Described in *Fusarium heterosporum* (Kakule et al. 2013) and *Fusarium graminearum* (Hegge et al. 2015), respectively, fusaridione A is a tetramic acid with reported antimicrobial activity, while fusaristatin A has shown *in vitro* activity against a lung-cancer cell line. *W. balasubramanianii* also harbored five homologs out of the nine components of the helvolic acid BGC characterized in *Aspergillus fumigatus*, which has previously demonstrated antibacterial activity (Lv et al. 2017).

P. burdickii likewise contained BGCs of biotechnological interest, including predicted pathways related to the production of duclauxin-like aromatic polyketides (Shahid et al. 2021) and usnic-acid-like compounds (Abdel-Hameed et al. 2016). Additionally, homologs of the oxidosqualene cyclase involved in the synthesis of clavaric acid were identified in four of the six candidate novel species (*W. balasubramanianii*, *C. crawfordii*, *P. burdickii*, and *S. californiae*). Clavaric acid is a fungal triterpenoid reported to inhibit farnesyl-protein transferase, an enzyme involved in oncogenic signaling, therefore of high biotechnological interest (Godio and Martín 2009).

Although BGC completeness and production of the predicted metabolites remain to be demonstrated, these results indicate a diverse repertoire of pathways related to the production of pigments, siderophores, and polyketides, which could potentially mediate competition, signaling, or stress protection and may have biotechnological value.

Predicted BGCs and Potential Crew or Habitat Risk

Mechanistic interpretation of predicted BGCs also served to identify potential associated risks to crew health and habitat. For example, *P. burdickii* encoded a close homolog of the cercosporin cluster in *Cercospora nicotianae* (Chen et al. 2007), previously isolated from members of the *Phaeophleospora* genus (Savi et al. 2018). Cercosporin is a photoactive compound that contributes to fungal virulence and oxidative-stress resistance (Chen et al. 2007). Cercosporin is toxic to a wide array of organisms including bacteria, mammals, plants, and most fungal species, with the key exception of cercosporin-producing fungi. In addition, *N. huberi* contained a close homolog of the experimentally characterized sterigmatocystin and aflatoxins B1/B2 cluster in *Aspergillus ochraceoroseus* (Cary et al. 2009). Although the present evidence is not sufficient to prove toxin production by *P. burdickii* and *N. huberi*, it helps identify and prioritize the risks associated with their persistence in controlled environments.

A Mechanistic Model for Persistence in Spacecraft and Planetary Habitats

Together, these observations support a model in which no single genomic trait explains the enhanced persistence of these fungi within the cleanrooms. Instead, persistence may have emerged from different combinations of, among others, pigmentation, enhanced metal acquisition and carbohydrate use, and signaling. These functions could be relevant to long-term missions, where microorganisms in closed or semi-closed habitats may be exposed to chronic low-dose radiation, desiccation, nutrient limitation, oxidative stress, and repeated cleaning on engineered surfaces.

The genomic and functional characterization of the seven isolates described in this study, integrated with independent cultivation and experimental evidence, provides a possible mechanistic interpretation of the enhanced persistence of these isolates. Demonstrating pathway expression, metabolite production, or causal contributions to their environmental persistence is beyond the taxonomic and comparative-genomic scope of the present study. The large percentage of uncharacterized proteins and functions indicate that the mechanisms undermining such persistence, however, remain vastly unexplored.

Conclusion

Integration of colony and cell morphology, multilocus phylogeny and genome-scale analyses supported the recognition of six previously uncharacterized fungal species represented by seven isolates recovered from Mars 2020 mission assembly cleanrooms. Using a set of 61 conserved protein-coding genes generally provided greater species-level resolution than ITS and LSU, underscoring the limitations of relying on ribosomal markers alone for fungal species identification. Comparative genomics further revealed variation in genome content, predicted functional traits and BGCs, suggesting diverse metabolic capacities among the isolates. Our findings expand knowledge of fungi capable of persisting in oligotrophic, stringently maintained facilities and demonstrate the value of genome-informed fungal surveillance. Improved detection and characterization of such fungi can strengthen microbial monitoring, contamination control and planetary-protection risk assessment for future NASA exploration missions and closed human habitats.

Statements and Declarations

The authors used ChatGPT (OpenAI) solely for language editing and improvement of clarity and readability. All scientific content, analyses, interpretations, and conclusions were developed and verified by the authors, who take full responsibility for the final manuscript.

Acknowledgements: The research was carried out at the Jet Propulsion Laboratory, California Institute of Technology, under a contract with the National Aeronautics and Space Administration (80NM0018D0004). © 2026 All rights reserved. We thank the members of the Biotechnology and Planetary Protection Group, particularly Cynthia Ly for sample collection and Ceth Parker for calibrating the scale bars in selected panels of Fig. 1. We would like to thank Snehit Mhatre for collecting the strains and primary identification using ITS as a diagnostic marker. DIC imaging was performed at California State Polytechnic University, Pomona, CA with the support of Wei-Jen Lin and Craig W. LaMunyon. We thank Zymo Corp. for extracting DNA, Dan Butler (Cornell Medicine) for performing shotgun sequencing using the NovaSeq platform. The funders had no role in study design, data collection and interpretation, the writing of the manuscript, or the decision to submit the work for publication.

Funding: The research described in this manuscript was funded by the NNH18ZDA001N-PPR award 18-PPR18-0011 to K.V. A.T. is supported by the Environmental Protection Agency Research Programme 2021-2030 as a Government of Ireland initiative funded by the Department of the

Environment, Climate and Communications, under grant number 2022-HE-1145. C.E.M. thanks the Scientific Computing Unit (SCU) at WCM, the WorldQuant and GI Research Foundation (GIRF), NASA (80NSSC24K0728, 80NSSC24K1052, 80NSSC25K7731), the National Institutes of Health (U54AG089334), Bumrungrad International Hospital, and Yekaterina Chudnovsky. We acknowledge Boryung for their financial support and research enhancement ground, provided through their Global Space Healthcare Initiative, Humans In Space, including mentorship and access to relevant expert networks.

Author Contributions: K.V. and N.K.S. conceived and designed the study. K.V. and A.M.C. designed and performed bright-field microscopy experiments. K.V. isolated the fungal strains. C.E.M. generated whole-genome shotgun sequencing data using the NovaSeq platform. M.d.M.T., E.J., and G.S. performed MLSA analyses and sequence alignments to determine the phylogenetic placement of the isolates. D.K. performed WGS-based phylogenetic analysis. A.M.C. and M.P.W. cultured and incubated all strains for phenotypic characterization and microscopy. M.P.W. performed differential interference contrast (DIC) microscopy, prepared annotated images with scale bars, and, together with T.T., A.M.C., and K.V. selected representative images and prepared morphological descriptions. M.d.M.T., A.T., G.M., and A.M.C. conducted genome analyses, including *de novo* assembly, assembly verification, scaffold quality assessment, genome annotation, and draft genome generation. A.M.C. submitted the genome assemblies to NCBI. A.M.C. prepared the initial manuscript draft, including the Introduction, Materials and Methods, Results, and Discussion. K.V. and A.M.C. coordinated manuscript preparation by integrating contributions on microscopy (M.P.W.), MLSA phylogenetic analyses and figure preparation (M.d.M.T., E.J., and G.S.), WGS phylogeny (D.K.), and genome characterization (A.T., N.K.S., and G.M.). All authors reviewed, revised, and approved the final manuscript.

Data availability: The genome assemblies generated in this study are available in GenBank under the BioProject and accession numbers provided in the manuscript (Table 1). Marker sequences retrieved from the WGS of the strains studied and other associated accession numbers are reported in the main text and supplementary materials (Table 1 and Supplemental File xx). Additional data are available from the corresponding author upon reasonable request.

Competing interests: The authors declare that they have no relevant financial or non-financial interests to disclose.

Ethics approval: This study involved environmental fungal isolates and did not involve human participants, human-derived identifiable material or live vertebrate animals. Ethical approval was therefore not required.

Consent to participate: Not applicable.

Consent for publication: Not applicable.

751 **References**

752 Abdel-Hameed M, Bertrand RL, Piercey-Normore MD, Sorensen JL (2016) Putative identification
753 of the usnic acid biosynthetic gene cluster by de novo whole-genome sequencing of a lichen-
754 forming fungus. Fungal Biology 120 (3):306-316. doi:10.1016/j.funbio.2015.10.009
755 Bahn YS, Xue C, Idnurm A, Rutherford JC, Heitman J, Cardenas ME (2007) Sensing the
756 environment: lessons from fungi. Nature Reviews Microbiology 5 (1):57-69.
757 doi:10.1038/nrmicro1578
758 Bankevich A, Nurk S, Antipov D, Gurevich AA, Dvorkin M, Kulikov AS, Lesin VM, Nikolenko SI,
759 Pham S, Prjibelski AD, Pyshkin AV, Sirotkin AV, Vyahhi N, Tesler G, Alekseyev MA,
760 Pevzner PA (2012) SPAdes: A New Genome Assembly Algorithm and Its Applications to
761 Single-Cell Sequencing. Journal of Computational Biology 19 (5):455-477.
762 doi:10.1089/cmb.2012.0021
763 Belizario JA, Lopes LG, Pires RH (2021) Fungi in the indoor air of critical hospital areas: a review.
764 Aerobiologia 37:379-394. doi:10.1007/s10453-021-09706-7
765 Benardini JN, 3rd, La Duc MT, Beaudet RA, Koukol R (2014) Implementing planetary protection
766 measures on the Mars Science Laboratory. Astrobiology 14 (1):27-32.
767 doi:10.1089/ast.2013.0989
768 Blachowicz A, Mhatre S, Singh NK, Wood JM, Parker CW, Ly C, Butler D, Mason CE,
769 Venkateswaran K (2022) The Isolation and Characterization of Rare Mycobiome Associated
770 With Spacecraft Assembly Cleanrooms. Front Microbiol 13:777133.
771 doi:10.3389/fmicb.2022.777133
772 Blin K, Shaw S, Vader L, Szenei J, Reitz ZL, Augustijn HE, Cediel-Becerra JDD, de Crécy-Lagard
773 V, Koetsier RA, Williams SE, Cruz-Morales P, Wongwas S, Segurado Luchsinger AE,
774 Biermann F, Korenskaia A, Zdouc MM, Meijer D, Terlouw BR, van der Hooft JJJ (2025)
775 antiSMASH 8.0: extended gene cluster detection capabilities and analyses of chemistry,
776 enzymology, and regulation. Nucleic acids research 53 (W1):W32-W38.
777 doi:10.1093/nar/gkaf334
778 Camacho C, Coulouris G, Avagyan V, Ma N, Papadopoulos J, Bealer K, Madden TL (2009)
779 BLAST+: architecture and applications. BMC bioinformatics 10 (1). doi:10.1186/1471-2105-
780 10-421
781 Cary JW, Ehrlich KC, Beltz SB, Harris-Coward P, Klich MA (2009) Characterization of the
782 *Aspergillus ochraceoroseus* aflatoxin/sterigmatocystin biosynthetic gene cluster. Mycologia 101
783 (3):352-362. doi:10.3852/08-173
784 Casadevall A, Cordero RJB, Bryan R, Nosanchuk J, Dadachova E (2017) Melanin, radiation, and
785 energy transduction in fungi. Microbiology spectrum 5:FUNK-0037-2016.
786 doi:10.1128/microbiolspec.FUNK-0037-2016
787 Chander AM, Burr DJ, Wipf S, Nitsche R, Fujimura G, Schubert W, Singh NK, Bell JJ, Brandl A,
788 Weil MM, Elsaesser A, Venkateswaran K (2026) Survival of NASA-cleanroom microbial
789 isolates under simulated space and Martian conditions. Applied and Environmental
790 Microbiology 0 (0):e02065-02025. doi:doi:10.1128/aem.02065-25
791 Chander AM, de Melo Teixeira M, Singh NK, Williams MP, Parker CW, Leo P, Stajich JE, Torok T,
792 Tighe S, Mason CE, Venkateswaran K (2024) Genomic and morphological characterization
793 of *Knufia obscura* isolated from the Mars 2020 spacecraft assembly facility. Scientific Reports
794 14 (1):12249. doi:10.1038/s41598-024-61115-1
795 Chander AM, Teixeira MdM, Singh NK, Williams MP, Simpson AC, Damle N, Parker CW, Stajich
796 JE, Mason CE, Torok T, Venkateswaran K (2023) Description and Genome
797 Characterization of Three Novel Fungal Strains Isolated from Mars 2020 Mission-Associated

798 Spacecraft Assembly Facility: Recommendations for Two New Genera and One Species.
799 Journal of Fungi 9 (1):31
800 Chen H, Lee MH, Daub ME, Chung KR (2007) Molecular analysis of the cercosporin biosynthetic
801 gene cluster in *Cercospora nicotianae*. Molecular Microbiology 64 (3):755-770.
802 doi:10.1111/j.1365-2958.2007.05689.x
803 Crous PW, Gams W, Stalpers JA, Robert V, Stegehuis G (2004) MycoBank: an online initiative to
804 launch mycology into the 21st century. Stud Mycol 50:19-22
805 Dijksterhuis J (2019) Fungal spores: highly variable and stress-resistant vehicles for distribution and
806 spoilage. Food Microbiology 81:2-11. doi:10.1016/j.fm.2018.11.006
807 Flynn JM, Hubley R, Goubert C, Rosen J, Clark AG, Feschotte C, Smit AF (2020) RepeatModeler2
808 for automated genomic discovery of transposable element families. Proceedings of the
809 National Academy of Sciences 117 (17):9451-9457. doi:10.1073/pnas.1921046117
810 Frith MC (2010) A new repeat-masking method enables specific detection of homologous
811 sequences. Nucleic acids research 39 (4):e23-e23. doi:10.1093/nar/gkq1212
812 Gabriel L, Brůna T, Hoff KJ, Ebel M, Lomsadze A, Borodovsky M, Stanke M (2024) BRAKER3:
813 Fully automated genome annotation using RNA-seq and protein evidence with GeneMark-
814 ETP, AUGUSTUS, and TSEBRA. Genome research 34 (5):769-777.
815 doi:10.1101/gr.278090.123
816 Gardes M, Bruns TD (1993) ITS primers with enhanced specificity for basidiomycetes - application
817 to the identification of mycorrhizae and rusts. Molecular Ecology 2 (2):113-118.
818 doi:10.1111/j.1365-294x.1993.tb00005.x
819 Godio RP, Martín JF (2009) Modified oxidosqualene cyclases in the formation of bioactive
820 secondary metabolites: Biosynthesis of the antitumor clavaric acid. Fungal Genetics and
821 Biology 46 (3):232-242. doi:10.1016/j.fgb.2008.12.002
822 Gostinčar C, Muggia L, Grube M (2012) Polyextremotolerant black fungi: oligotrophism, adaptive
823 potential, and a link to lichen symbioses. Frontiers in microbiology 3:390.
824 doi:10.3389/fmicb.2012.00390
825 Guindon S, Dufayard J-F, Lefort V, Anisimova M, Hordijk W, Gascuel O (2010) New Algorithms
826 and Methods to Estimate Maximum-Likelihood Phylogenies: Assessing the Performance of
827 PhyML 3.0. Systematic Biology 59 (3):307-321. doi:10.1093/sysbio/syq010
828 Gurevich A, Saveliev V, Vyahhi N, Tesler G (2013) QUAST: quality assessment tool for genome
829 assemblies. Bioinformatics 29 (8):1072-1075. doi:10.1093/bioinformatics/btt086
830 Hegge A, Lønborg R, Nielsen DM, Sørensen JL (2015) Factors influencing production of
831 fusaristatin A in *Fusarium graminearum*. Metabolites 5 (2):184-191.
832 doi:10.3390/metabo5020184
833 Hoang DT, Chernomor O, von Haeseler A, Minh BQ, Vinh LS (2017) UFBoot2: Improving the
834 Ultrafast Bootstrap Approximation. Molecular Biology and Evolution 35 (2):518-522.
835 doi:10.1093/molbev/msx281
836 Kakule TB, Sardar D, Lin Z, Schmidt EW (2013) Two related pyrrolidinedione synthetase loci in
837 Fusarium heterosporum ATCC 74349 produce divergent metabolites. ACS Chemical
838 Biology 8 (7):1549-1557. doi:10.1021/cb400159f
839 Kalyaanamoorthy S, Minh BQ, Wong TKF, von Haeseler A, Jermiin LS (2017) ModelFinder: fast
840 model selection for accurate phylogenetic estimates. Nature methods 14 (6):587-589.
841 doi:10.1038/nmeth.4285
842 Katoh K, Standley DM (2013) MAFFT multiple sequence alignment software version 7:
843 improvements in performance and usability. Mol Biol Evol 30. doi:10.1093/molbev/mst010

844 Kawai M, Ichijo T, Takahashi Y, Noguchi M, Katayama H, Cho O, Sugita T, Nasu M (2019)
845 Culture-independent approach reveals domination of human-oriented microbes in a
846 pharmaceutical manufacturing facility. Eur J Pharm Sci 137:104973.
847 doi:10.1016/j.ejps.2019.104973
848 Keller NP (2019) Fungal secondary metabolism: regulation, function and drug discovery. Nature
849 Reviews Microbiology 17:167-180. doi:10.1038/s41579-018-0121-1
850 Kim D, Gilchrist CLM, Chun J, Steinegger M (2022) UFCG: database of universal fungal core genes
851 and pipeline for genome-wide phylogenetic analysis of fungi. Nucleic acids research 51
852 (D1):D777-D784. doi:10.1093/nar/gkac894
853 Krasnoff SB, Keresztes I, Donzelli BGG, Gibson DM (2014) Metachelins, Mannosylated and N-
854 Oxidized Coprogen-Type Siderophores from *Metarhizium robertsii*. Journal of natural
855 products 77 (7):1685-1692. doi:10.1021/np500300s
856 La Duc MT, Vaishampayan P, Nilsson HR, Torok T, Venkateswaran K (2012) Pyrosequencing-
857 derived bacterial, archaeal, and fungal diversity of spacecraft hardware destined for Mars.
858 Appl Environ Microbiol 78 (16):5912-5922. doi:AEM.01435-12 [pii] 10.1128/AEM.01435-
859 12
860 Leach MD, Klipp E, Cowen LE, Brown AJP (2012) Fungal Hsp90: a biological transistor that tunes
861 cellular outputs to thermal inputs. Nature Reviews Microbiology 10 (10):693-704.
862 doi:10.1038/nrmicro2875
863 Leck A (1999) Preparation of lactophenol cotton blue slide mounts. Community Eye Health 12:24
864 Lopes AMM, Félix de Mélo AH, Procópio DP, Teixeira GS, Carazzolle MF, de Carvalho LM,
865 Adelantado N, Pereira GAG, Ferrer P, Maugeri Filho F, Goldbeck R (2020) Genome
866 sequence of Acremonium strictum AAJ6 strain isolated from the Cerrado biome in Brazil
867 and CAZymes expression in thermotolerant industrial yeast for ethanol production. Process
868 Biochemistry 98:139-150. doi:10.1016/j.procbio.2020.07.029
869 Lücking R, Aime MC, Robbertse B, Miller AN, Ariyawansa HA, Aoki T, Cardinali G, Crous PW,
870 Druzhinina IS, Geiser DM, Hawksworth DL, Hyde KD, Irinyi L, Jeewon R, Johnston PR,
871 Kirk PM, Malosso E, May TW, Meyer W, Öpik M, Robert V, Stadler M, Thines M, Vu D,
872 Yurkov AM, Zhang N, Schoch CL (2020) Unambiguous identification of fungi: where do we
873 stand and how accurate and precise is fungal DNA barcoding? IMA Fungus 11 (1):14.
874 doi:10.1186/s43008-020-00033-z
875 Lv JM, Hu D, Gao H, Kushiro T, Awakawa T, Chen GD, Wang CX, Abe I, Yao XS (2017)
876 Biosynthesis of helvolic acid and identification of an unusual C-4-demethylation process
877 distinct from sterol biosynthesis. Nature Communications 8:1644. doi:10.1038/s41467-017-
878 01813-9
879 Ma R, Huang H, Bai Y, Luo H, Fan Y, Yao B (2018) Insight into the cold adaptation and
880 hemicellulose utilization of *Cladosporium neopsychrotolerans* from genome analysis and
881 biochemical characterization. Scientific Reports 8:6075. doi:10.1038/s41598-018-24443-7
882 Minh BQ, Hahn MW, Lanfear R (2020) New Methods to Calculate Concordance Factors for
883 Phylogenomic Datasets. Molecular Biology and Evolution 37 (9):2727-2733.
884 doi:10.1093/molbev/msaa106
885 Mirarab S, Nguyen N, Guo S, Wang LS, Kim J, Warnow T (2014) PASTA: Ultra-Large Multiple
886 Sequence Alignment for Nucleotide and Amino-Acid Sequences. Journal of Computational
887 Biology 22 (5):377-386. doi:10.1089/cmb.2014.0156
888 Moissl-Eichinger C, Auerbach AK, Probst AJ, Mahnert A, Tom L, Piceno Y, Andersen GL,
889 Venkateswaran K, Rettberg P, Barczyk S, Pukall R, Berg G (2015) Quo vadis? Microbial
890 profiling revealed strong effects of cleanroom maintenance and routes of contamination in
891 indoor environments. Scientific Reports 5 (1):9156. doi:10.1038/srep09156

892 Nilsson RH, Anslan S, Bahram M, Wurzbacher C, Baldrian P, Tedersoo L (2019) Mycobiome
893 diversity: high-throughput sequencing and identification of fungi. Nature Reviews
894 Microbiology 17 (2):95-109. doi:10.1038/s41579-018-0116-y
895 Oh Y, Donofrio N, Pan H, Coughlan S, Brown DE, Meng S, Mitchell T, Dean RA (2008)
896 Transcriptome analysis reveals new insight into appressorium formation and function in the
897 rice blast fungus *Magnaporthe oryzae*. Genome biology 9 (5). doi:10.1186/gb-2008-9-5-r85
898 Parker CW, Teixeira MdM, Singh NK, Raja HA, Cank KB, Spigolon G, Oberlies NH, Barker BM,
899 Stajich JE, Mason CE, Venkateswaran K (2022) Genomic Characterization of *Parengyodontium*
900 *torokii* sp. nov., a Biofilm-Forming Fungus Isolated from Mars 2020 Assembly Facility.
901 Journal of Fungi 8 (1):66
902 Patel RK, Jain M (2012) NGS QC Toolkit: A Toolkit for Quality Control of Next Generation
903 Sequencing Data. PLoS ONE 7 (2):e30619. doi:10.1371/journal.pone.0030619
904 Pope RE, Prade RA (2026) Vesicle-driven endomembrane systems in fungi. Microbiology and
905 Molecular Biology Reviews 90 (1). doi:10.1128/mmbr.00297-24
906 Qin Y, Lu H, Qi X, Lin M, Gao C, Liu Y, Luo X (2024) Recent Advances in Chemistry and
907 Bioactivities of Secondary Metabolites from the Genus Acremonium. Journal of Fungi 10
908 (1):37. doi:10.3390/jof10010037
909 Quaedvlieg W, Binder M, Groenewald JZ, Summerell BA, Carnegie AJ, Burgess TI, Crous PW
910 (2014) Introducing the Consolidated Species Concept to resolve species in the
911 Teratosphaeriaceae. Persoonia 33:1-40. doi:10.3767/003158514X681981
912 Riddel RW (1950) Permanent stained mycological preparations obtained by slide culture. Mycologia
913 42:265-270. doi:10.1080/00275514.1950.12017830
914 Roy A, Tamuli R (2022) Heat shock proteins and the calcineurin-crz1 signaling regulate stress
915 responses in fungi. Archives of microbiology 204 (5). doi:10.1007/s00203-022-02833-w
916 Sandle T (2021) Study of fungi isolated from pharmaceutical cleanrooms: types and origins.
917 European Journal of Parenteral and Pharmaceutical Sciences 26 (2)
918 Savi DC, Shaaban KA, Gos FMWR, Ponomareva LV, Thorson JS, Glienke C, Rohr J (2018)
919 *Phaeophleospora vochysiae* Savi & Glienke sp. nov. isolated from Vochysia divergens found in
920 the Pantanal, Brazil, produces bioactive secondary metabolites. Scientific Reports 8:3122.
921 doi:10.1038/s41598-018-21400-2
922 Sayers EW, Cavanaugh M, Clark K, Pruitt KD, Sherry ST, Yankie L, Karsch-Mizrachi I (2023)
923 GenBank 2024 Update. Nucleic acids research 52 (D1):D134-D137.
924 doi:10.1093/nar/gkad903
925 Schoch CL, Seifert KA, Huhndorf S, Robert V, Spouge JL, Levesque CA, Chen W, Bolchacova E,
926 Voigt K, Crous PW, Miller AN, Wingfield MJ, Aime MC, An K-D, Bai F-Y, Barreto RW,
927 Begerow D, Bergeron M-J, Blackwell M, Boekhout T, Bogale M, Boonyuen N, Burgaz AR,
928 Buyck B, Cai L, Cai Q, Cardinali G, Chaverri P, Coppins BJ, Crespo A, Cubas P, Cummings
929 C, Damm U, de Beer ZW, de Hoog GS, Del-Prado R, Dentinger B, Diéguez-Uribeondo J,
930 Divakar PK, Douglas B, Dueñas M, Duong TA, Eberhardt U, Edwards JE, Elshahed MS,
931 Fliegerova K, Furtado M, García MA, Ge Z-W, Griffith GW, Griffiths K, Groenewald JZ,
932 Groenewald M, Grube M, Gryzenhout M, Guo L-D, Hagen F, Hambleton S, Hamelin RC,
933 Hansen K, Harrold P, Heller G, Herrera C, Hirayama K, Hirooka Y, Ho H-M, Hoffmann
934 K, Hofstetter V, Högnabba F, Hollingsworth PM, Hong S-B, Hosaka K, Houbraken J,
935 Hughes K, Huhtinen S, Hyde KD, James T, Johnson EM, Johnson JE, Johnston PR, Jones
936 EBG, Kelly LJ, Kirk PM, Knapp DG, Kõljalg U, Kovács GM, Kurtzman CP, Landvik S,
937 Leavitt SD, Liggenstoffer AS, Liimatainen K, Lombard L, Luangsa-ard JJ, Lumbsch HT,
938 Maganti H, Maharachchikumbura SSN, Martin MP, May TW, McTaggart AR, Methven AS,
939 Meyer W, Moncalvo J-M, Mongkolsamrit S, Nagy LG, Nilsson RH, Niskanen T, Nyilasi I,

940 Okada G, Okane I, Olariaga I, Otte J, Papp T, Park D, Petkovits T, Pino-Bodas R,
941 Quaedvlieg W, Raja HA, Redecker D, Rintoul TL, Ruibal C, Sarmiento-Ramírez JM, Schmitt
942 I, Schüßler A, Shearer C, Sotome K, Stefani FOP, Stenroos S, Stielow B, Stockinger H,
943 Suetrong S, Suh S-O, Sung G-H, Suzuki M, Tanaka K, Tedersoo L, Telleria MT, Tretter E,
944 Untereiner WA, Urbina H, Vágvölgyi C, Vialle A, Vu TD, Walther G, Wang Q-M, Wang Y,
945 Weir BS, Weiß M, White MM, Xu J, Yahr R, Yang ZL, Yurkov A, Zamora J-C, Zhang N,
946 Zhuang W-Y, Schindel D (2012) Nuclear ribosomal internal transcribed spacer (ITS) region
947 as a universal DNA barcode marker for Fungi. Proceedings of the National Academy of
948 Sciences 109 (16):6241-6246. doi:doi:10.1073/pnas.1117018109
949 Scholz MB, Lo C-C, Chain PSG (2012) Next generation sequencing and bioinformatic bottlenecks:
950 the current state of metagenomic data analysis. Current opinion in biotechnology 23 (1):9-15.
951 doi:http://dx.doi.org/10.1016/j.copbio.2011.11.013
952 Shahid H, Cai T, Wang Y, Zheng C, Yang Y, Mao Z, Ding P, Shan T (2021) Duclauxin derivatives
953 from fungi and their biological activities. Frontiers in microbiology 12:766440.
954 doi:10.3389/fmicb.2021.766440
955 Shoji J, Kikuma T, Kitamoto K (2014) Vesicle trafficking, organelle functions, and unconventional
956 secretion in fungal physiology and pathogenicity. Current Opinion in Microbiology 20:1-9.
957 doi:10.1016/j.mib.2014.03.002
958 Steenwyk JL, Buida TJ, III, Li Y, Shen X-X, Rokas A (2020) ClipKIT: A multiple sequence
959 alignment trimming software for accurate phylogenomic inference. PLOS Biology 18
960 (12):e3001007. doi:10.1371/journal.pbio.3001007
961 Stielow JB, Lévesque CA, Seifert KA, Meyer W, Irinyi L, Smits D, Renfurm R, Verkley GJM,
962 Groenewald M, Chaduli D, Lomascolo A, Welti S, Lesage-Meessen L, Favel A, Al-Hatmi
963 AMS, Damm U, Yilmaz N, Houbraken J, Lombard L (2015) One fungus, which genes?
964 Development and assessment of universal primers for potential secondary fungal DNA
965 barcodes. Persoonia - Molecular Phylogeny and Evolution of Fungi 35 (1):242-263.
966 doi:10.3767/003158515x689135
967 Tan YP, Minns SA, Crombie A, Smith PJ, Lacey E (2024): Index of Australian Fungi no. 42. In., v1
968 edn: Zenodo. Doi: 10.5281/zenodo.13231264
969 Tarailo-Graovac M, Chen N (2009) Using RepeatMasker to Identify Repetitive Elements in
970 Genomic Sequences. Current Protocols in Bioinformatics 25 (1).
971 doi:10.1002/0471250953.bi0410s25
972 Taylor DL, Bruns TD (1999) Community structure of ectomycorrhizal fungi in a *Pinus muricata*
973 forest: minimal overlap between the mature forest and resistant propagule communities. Mol
974 Ecol 8. doi:10.1046/j.1365-294x.1999.00773.x
975 Taylor JW, Jacobson DJ, Kroken S, Kasuga T, Geiser DM, Hibbett DS, Fisher MC (2000)
976 Phylogenetic species recognition and species concepts in fungi. Fungal Genet Biol 31 (1):21-
977 32. doi:10.1006/fgbi.2000.1228
978 Tegenfeldt F, Kuznetsov D, Manni M, Berkeley M, Zdobnov EM, Kriventseva EV (2024) OrthoDB
979 and BUSCO update: annotation of orthologs with wider sampling of genomes. Nucleic acids
980 research 53 (D1):D516-D522. doi:10.1093/nar/gkae987
981 Terfehr D, Dahlmann TA, Specht T, Zadra I, Kürnsteiner H, Kück U (2014) Genome sequence and
982 annotation of *Acremonium chrysogenum*, producer of the β-lactam antibiotic cephalosporin C.
983 Genome announcements 2 (5):e00948-00914. doi:10.1128/genomeA.00948-14
984 Tršan M, Seme K, Srčič S (2019) The environmental monitoring in hospital pharmacy cleanroom
985 and microbiota catalogue preparation. Saudi Pharmaceutical Journal 27 (4):455-462.
986 doi:https://doi.org/10.1016/j.jsps.2019.01.007

Walker BJ, Abeel T, Shea T, Priest M, Abouelliel A, Sakthikumar S, Cuomo CA, Zeng Q, Wortman J, Young SK, Earl AM (2014) Pilon: An Integrated Tool for Comprehensive Microbial Variant Detection and Genome Assembly Improvement. PLoS ONE 9 (11):e112963. doi:10.1371/journal.pone.0112963

Wisecaver JH, Rokas A (2015) Fungal metabolic gene clusters—caravans traveling across genomes and environments. Frontiers in microbiology 6:161. doi:10.3389/fmicb.2015.00161

Wong TKF, Ly-Trong N, Ren H, Demotte P, Baños H, Roger AJ, Susko E, Bielow C, De Maio N, Goldman N, Hahn MW, dos Reis M, Vinh LS, Huttley G, Lanfear R, Minh BQ (2026) IQ-TREE 3: phylogenomic inference software using complex evolutionary models. Molecular Biology and Evolution 43 (5). doi:10.1093/molbev/msag117

Yew SM, Chan CL, Ngeow YF, Toh YF, Na SL, Lee KW, Hoh CC, Yee WY, Ng KP (2016) Insight into different environmental niche adaptations and allergenicity from the Cladosporium sphaerospermum genome. Scientific Reports 6:27008. doi:10.1038/srep27008

Zhang J, Zhang P, Zeng G, Wu G, Qi L, Chen G, Fang W, Yin WB (2021) Transcriptional differences guided discovery and genetic identification of coprogen and dimerumic acid siderophores in *Metarhizium robertsii*. Frontiers in microbiology 12:783609. doi:10.3389/fmicb.2021.783609

Zhang P, Wang X, Fan A, Zheng Y, Liu X, Wang S, Zou H, Oakley BR, Keller NP, Yin WB (2017) A cryptic pigment biosynthetic pathway uncovered by heterologous expression is essential for conidial development in *Pestalotiopsis fici*. Molecular Microbiology 105 (3):469-483. doi:10.1111/mmi.13711

Figure legends

Figure 1. Colony and cell morphology of six novel fungal species isolated from NASA spacecraft assembly cleanroom environments. Rows represent: **1-1**, *Cladosporium prattiae* FJI-L7-BK-DG1^T; **1-2**, *Cladosporium crawfordii* FJII-L10-SW-DR1^T; **1-3**, *Waltergamsia balasubramanianii* FKII-L8-BK-P5^T; **1-4**, *Phaeophleospora burdickii* FKII-L3-CM-PAB3^T; **1-5**, *Spissiomyces californiae* FJII-L1-SW-P2^T; and **1-6**, *Neocatenulostroma huberi* FJI-L3-BK-P2^T. **Column A** shows colony morphology on PDA for 1-1 through 1-4 and 1-6, and on OMA for *S. californiae* (1-5). **Columns B and C** show representative DIC micrographs illustrating hyphal and reproductive structures of the respective isolates. Scale bars are indicated within the individual micrographs.

Figure 2. Multilocus sequence analysis (*ITS, tef1-α, act, rpb2,* and *tub2*) of *Cladosporium prattiae* FJI-L7-BK-DG1^T and related *Cladosporium* taxa. Phylogenetic placement of *C. prattiae* FJI-L7-BK-DG1^T was inferred from concatenated multilocus sequence data and is highlighted in red. Reference taxa, including type strains (T), are shown in black. Numerical values at internal nodes indicate branch-support values. The scale bar represents 0.02 substitutions per site.

Figure 3. Whole-genome phylogenomic placement of six novel fungal species recovered from NASA Mars 2020 spacecraft assembly environments. Whole-genome phylogenomic analysis used a standardized set of 61 universal fungal core genes for genome-scale phylogenetic inference (Kim et al. 2022). The analysis included 81 publicly available whole-genome assemblies representing 81 Ascomycota species selected from the NCBI GenBank reference genome database (Sayers et al. 2024) to encompass the taxonomic neighborhoods of the novel isolates, together with representatives of *Aureobasidium* and *Trichoderma* and outgroup taxa from Saccharomycotina and Pezizomycetes. The six novel species, represented by seven genomes, are highlighted in color: *Acremonium balasubramanianii* FKII-L8-BK-P5^T, *Spissiomyces californiae* FJII-L1-SW-P2^T, *Phaeophleospora burdickii* FKII-L3-CM-PAB3^T, *Neocatenulostroma huberi* FJI-L3-BK-P2^T, *Cladosporium prattiae* FJI-L7-BK-DG1^T, and *Cladosporium crawfordii* FJII-L10-SW-DR1^T and FKII-L3-CM-PAB1. The 61-core-gene phylogeny resolves the novel taxa within their respective higher-level lineages, including Sordariomycetes and Dothideomycetes, while the two independently recovered *C. crawfordii* strains form a closely associated genomic lineage.

Figure 4. Multilocus sequence analysis (*ITS, tef1-α,* and *act*) of *Cladosporium crawfordii* FKII-L3-CM-PAB1^T and related *Cladosporium* taxa. Phylogenetic placement of *C. crawfordii* FKII-L3-CM-PAB1^T was inferred from concatenated multilocus sequence data and is highlighted in red. Reference taxa, including type strains (T), are shown in black. Numerical values at internal nodes indicate branch-support values from the respective phylogenetic analyses. The scale bar represents 0.03 substitutions per site.

Figure 5. Multilocus sequence analysis (*ITS, LSU, rpb2,* and *tef1-α*) of *Waltergamsia balasubramanianii* FKII-L8-BK-P5^T and phylogenetically related taxa. Phylogenetic placement of *W. balasubramanianii* FKII-L8-BK-P5^T was inferred from concatenated multilocus sequence data and is highlighted in red. Reference taxa and strains, including available type strains (T), are shown in black. Numerical values at internal nodes indicate branch-support values from the respective phylogenetic analyses. The scale bar represents 0.03 substitutions per site.

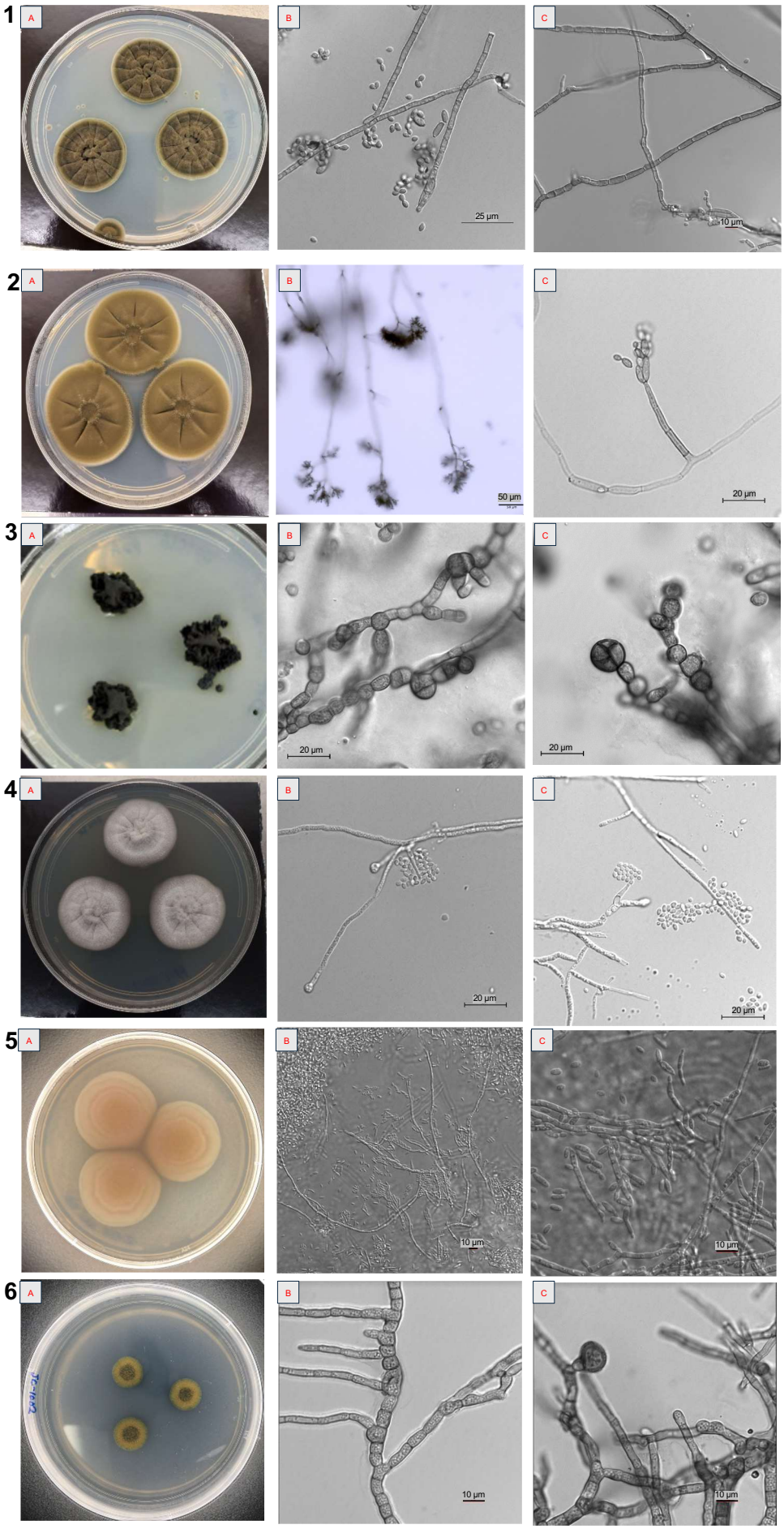
Figure 6 Phylogenetic placement of *Phaeophleospora burdickii* FKII-L3-CM-PAB3 (*ITS, LSU,* and *tef1-α*) among selected *Phaeophleospora* species. The proposed species was recovered as sister to the clade comprising *P. concentrica* and *P. indica*. The tree was rooted with *Lecanosticta acicola* CBS 133791 (WPF13.12). Node-support values were indicated beside the

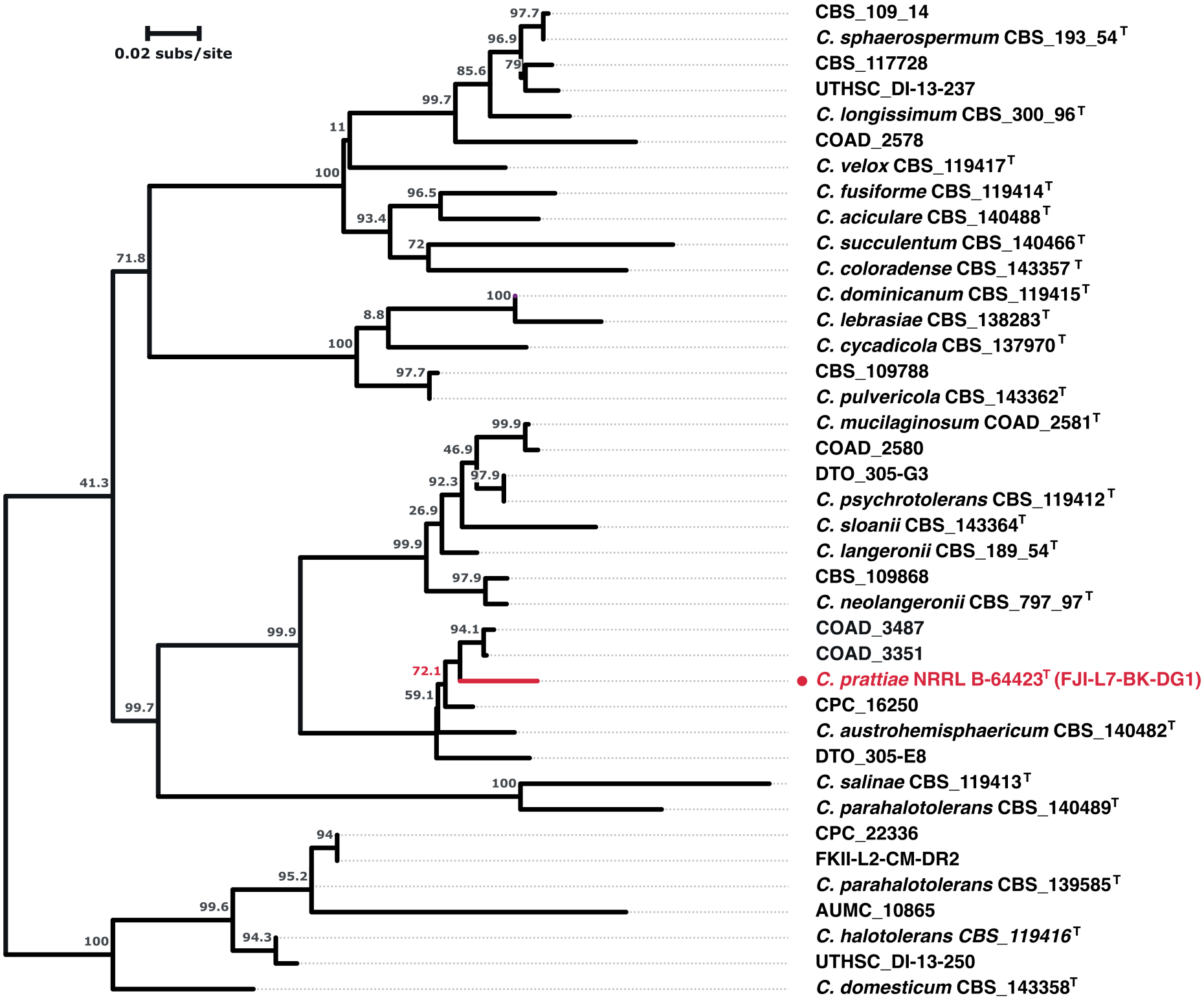
branches, and strains designated as type-derived were marked with a superscript T. Branch lengths were scaled to nucleotide substitutions per site; the scale bar represented 0.10 substitutions per site.

Figure 7 Phylogenetic placement of *Spissiomyces californiae* FJII-L1-SW-P2 (*ITS, LSU, SSU, rpb2,* and *tub2*) among selected related taxa. The proposed species was highlighted in red and was recovered as sister to the clade containing *S. endophytica*, *Neospissiomyces floridanus*, *S. ramosus*, *S. aggregatus* and two isolates *Dothideomycetes* sp. (CGMCC 3.17079 and CGMCC 3.17080). A support value of 100 was indicated at the node joining the proposed species and this clade. The tree was rooted with *A. megaspermum* AFTOL-ID 2094. Node-support values were indicated beside the branches, and strains designated as type-derived were marked with a superscript T. Branch lengths were scaled to nucleotide substitutions per site; the scale bar represented 0.20 substitutions per site.

Figure 8. Multilocus sequence analysis (*ITS, LSU, tef1-α, rpb2,* and *tub2*) of *Neocatenulostroma huberi* FJI-L3-BK-P2^T and phylogenetically related taxa. Phylogenetic placement of *N. huberi* FJI-L3-BK-P2^T was inferred from concatenated multilocus sequence data and is highlighted in red. Reference taxa and strains, including available type strains (T), are shown in black. Numerical values at internal nodes indicate branch-support values from the respective phylogenetic analyses. The scale bar represents 0.03 substitutions per site.

Figure 9. Functional repertoire of seven fungal isolates recovered from Mars 2020 spacecraft assembly environments. (A) Carbohydrate-active enzyme (CAZyme) profiles showing copy-number distributions of individual CAZyme families (heatmap) and the overall representation of auxiliary activities (AA), carbohydrate-binding modules (CBM), carbohydrate esterases (CE), glycoside hydrolases (GH), glycosyltransferases (GT), and polysaccharide lyases (PL) across the seven genomes. **(B)** MEROPS peptidase profiles showing the distribution and copy number of individual peptidase families (heatmap) and the overall abundance of aspartic, cysteine, glutamic, metallo, mixed, serine, and threonine peptidases and protease inhibitors. **(C)** Distribution of predicted proteins among COG functional categories, including functions associated with metabolism, cellular processes and signaling, and information storage and processing. COG category abbreviations are indicated in the figure. **(D)** Non-metric multidimensional scaling (NMDS) ordination based on Bray–Curtis dissimilarities of Pfam domain profiles, illustrating differences in overall protein-domain composition among the seven fungal genomes (stress = 0.0079).


1
A
B
25 µm
C
10 µm
2
A
B
50 µm
C
20 µm
3
A
B
20 µm
C
20 µm
4
A
B
20 µm
C
20 µm
5
A
B
10 µm
C
10 µm
6
A
B
10 µm
C
10 µm


0.02 subs/site
97.7
96.9
85.6
79
99.7
11
100
96.5
93.4
72
71.8
100
8.8
100
97.7
99.9
46.9
97.9
92.3
41.3
26.9
99.9
97.9
99.9
94.1
72.1
59.1
99.7
100
94
95.2
99.6
94.3
100
CBS_109_14
C. sphaerospermum CBS_193_54T
CBS_117728
UTHSC_DI-13-237
C. longissimum CBS_300_96T
COAD_2578
C. velox CBS_119417T
C. fusiforme CBS_119414T
C. aciculare CBS_140488T
C. succulentum CBS_140466T
C. coloradense CBS_143357T
C. dominicanum CBS_119415T
C. lebrasiae CBS_138283T
C. cycadicola CBS_137970T
CBS_109788
C. pulvericola CBS_143362T
C. mucilaginosum COAD_2581T
COAD_2580
DTO_305-G3
C. psychrotolerans CBS_119412T
C. sloanii CBS_143364T
C. langeronii CBS_189_54T
CBS_109868
C. neolangeronii CBS_797_97T
COAD_3487
COAD_3351
C. prattiae NRRL B-64423T (FJI-L7-BK-DG1)
CPC_16250
C. austrohemisphaericum CBS_140482T
DTO_305-E8
C. salinae CBS_119413T
C. parahalotolerans CBS_140489T
CPC_22336
FKII-L2-CM-DR2
C. parahalotolerans CBS_139585T
AUMC_10865
C. halotolerans CBS_119416T
UTHSC_DI-13-250
C. domesticum CBS_143358T

Wickerhamiella allomyrinae CBS 13167
Phaffomyces coquimbonensis CBS 12348
Saccharomyces cerevisiae S288C
Rhizina undulata CMW412
Choiromyces venosus 120613-1
Morchella disparilis PhC 293
Trichoderma orchidacearum COAD 3006
Trichoderma afroharzianum
Trichoderma chlorosporum CBS 114231
Emericellopsis terricola NRRL 54109
Hapsidospora chrysogena CGMCC3.3795
***Acremonium balasubramanianii* FKII-L8-BK-P5^{T}**
Geosmithia putterillii
Geosmithia flava
Acremonium polychromum NFCCI 6138
Gliomastix tumulicola JCM 17184
Clonostachys chuyangsinensis YFCC 8591
Clonostachys compactiuscula YFCC 8592
Clonostachys rogersoniana YFCC 895
Clonostachys solani
Clonostachys rhizophaga CGMCC3.3657
Clonostachys chloroleuca Cc878
Clonostachys byssicola
Clonostachys rosea NF-06
Coniosporium uncinatum CCFEE 5737
***Spissiomyces californiae* FJII-L1-SW-P2^{T}**
Lasiodiplodia brasiliensis LaRA1
Diplodia mutila CBS 112553
Neoscytalidium dimidiatum ND8
Macrophomina euphorbiicola ARM498
Trypethelium eluteriae
Bathelium mastoideum
Astrothelium macrocarpum
Bathelium carolinianum
Cryomyces minteri CCFEE 5187
Aureobasidium castaneae ZX033
Aureobasidium uvarum
Aureobasidium zeae 15JLMHKDK516
***Phaeophleospora burdickii* FKII-L3-CM-PAB3^{T}**
Nothopassalora personata LLS Mitchell 2
Exutisphaerella laricina CBS 326.52
Ramularia vizellae
Ramularia endophylla CBS 113265
Pseudocercospora ulei GCL012
Septoria astericola
Cercospora janseana RL44
Cercospora nicotianae 1110
Cercospora zeae-maydis LN
Teratosphaeria destructans CMW45982
Teratosphaeria epicoccoides CMW31933
Salinomyces thailandicus CCFEE 6315
Oleoguttula mirabilis CCFEE 5522
Meristemomyces frigidus CCFEE 5501
***Neocatenulostroma huberi* FJI-L3-BK-P2^{T}**
Acidiella bohemica
Catenulostroma hermanusense GZ55-1
Elasticomyces elasticus CCFEE 5806
Friedmanniomyces endolithicus CCFEE 5001
Rachicladosporium monterosium CCFEE 5386
Cryoendolithus antarcticus CCFEE 5527
Cladosporium fusiforme IBT 42164
Cladosporium sphaerospermum R2409
Cladosporium endophyticum LH A213
Cladosporium dominicanum ZJUC76
Cladosporium lebrasiae ZJUC516
***Cladosporium pratiae* FJI-L7-BK-DG1^{T}**
Cladosporium ramotenellum ZJUC95
Cladosporium phlei ATCC 36193
Cladosporium allicinum IBT 42152
Cladosporium subtilissimum
Cladosporium xanthochromaticum ZJUC393
***Cladosporium crawfordii* FJII-L10-SW-DR1^{T}**
***Cladosporium crawfordii* FKII-L3-CM-PAB1**
Cladosporium asperulatum ZJUC90
Cladosporium xylophilum F42
Graphiopsis chlorocephala
Cladosporium rectoides A179
Cladosporium pseudocladosporioides F105
Cladosporium inversicolor IBT 42153
Cladosporium europaeum F32
Cladosporium subuliforme ZJUC123
Cladosporium oxysporum AAAS A1
Cladosporium tenuissimum ACCC 37043
Cladosporium cucumerinum C1
Cladosporium velox C4
Cladosporium cladosporioides SYC63
Cladosporium colombiae 601
Cladosporium anthropophilum ZJUC72

0.2

Outgroup
Saccharomycotina

Outgroup
Pezizomycetes

Family
Bionectriaceae

Dothideomycetes
incerta sedis

Family
Mycosphaerellaceae

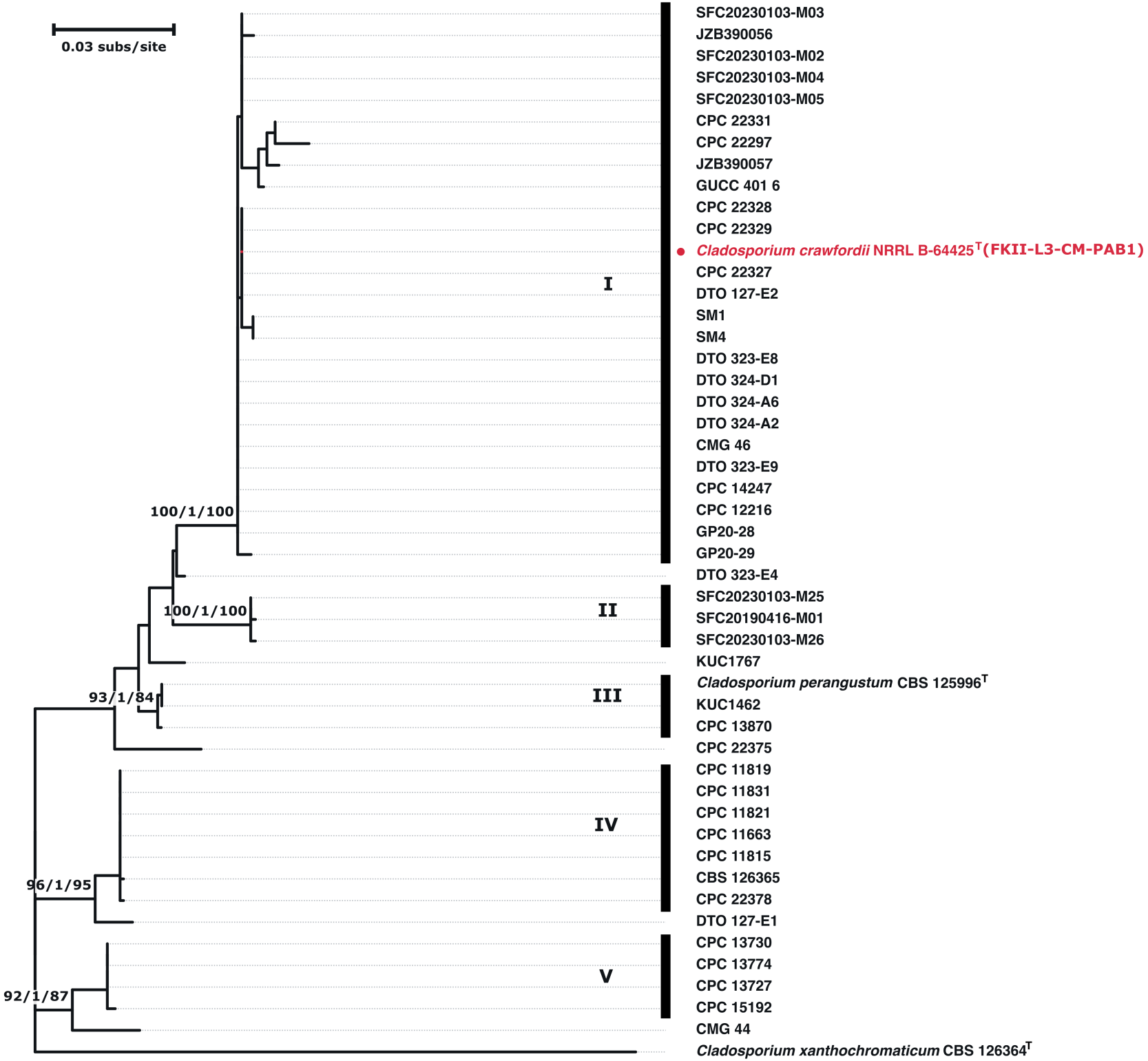
Family
Teratosphaeriaceae

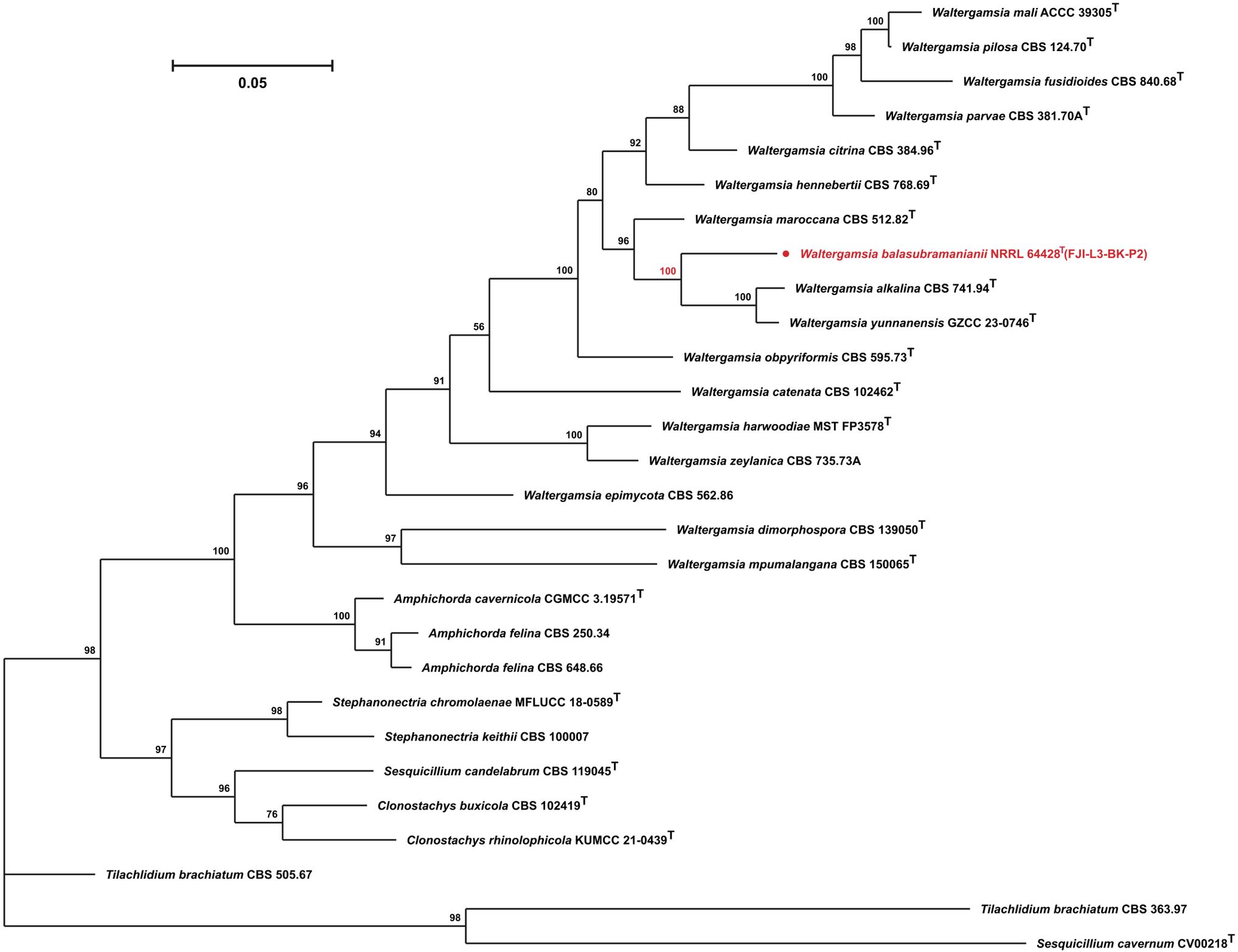
Family
Cladosporiaceae

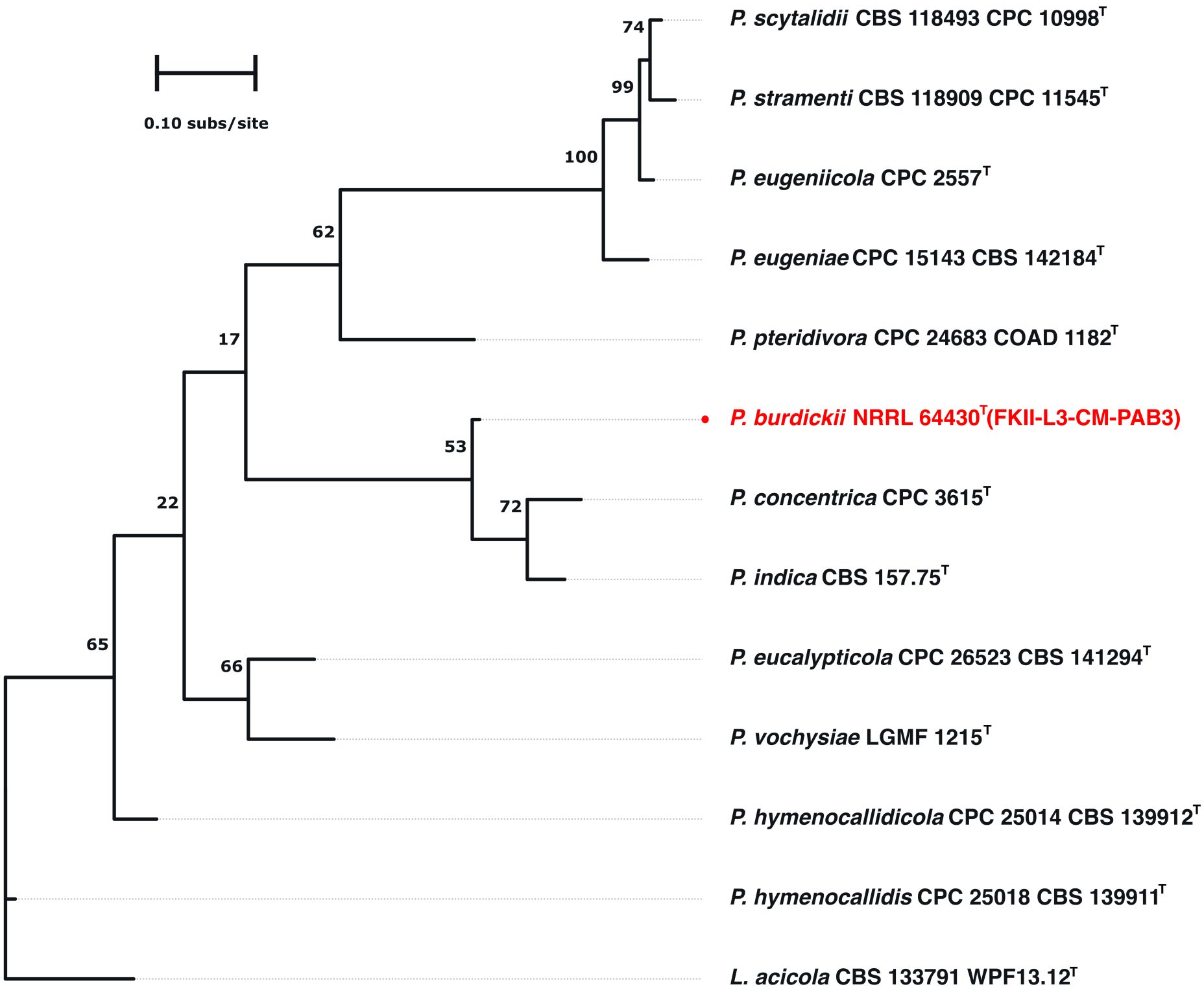
Class
Sordariomycetes

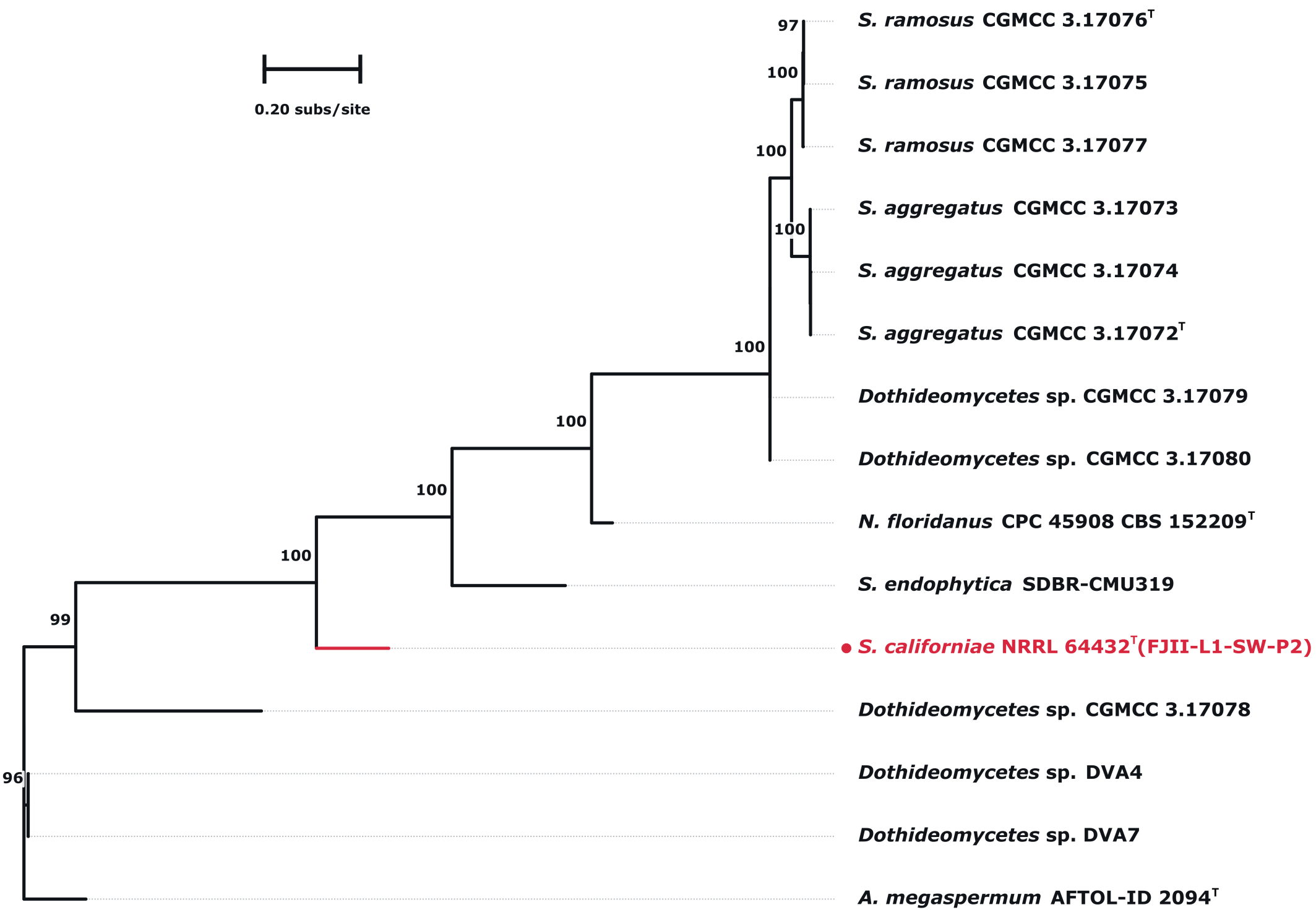
Class
Dothideomycetes

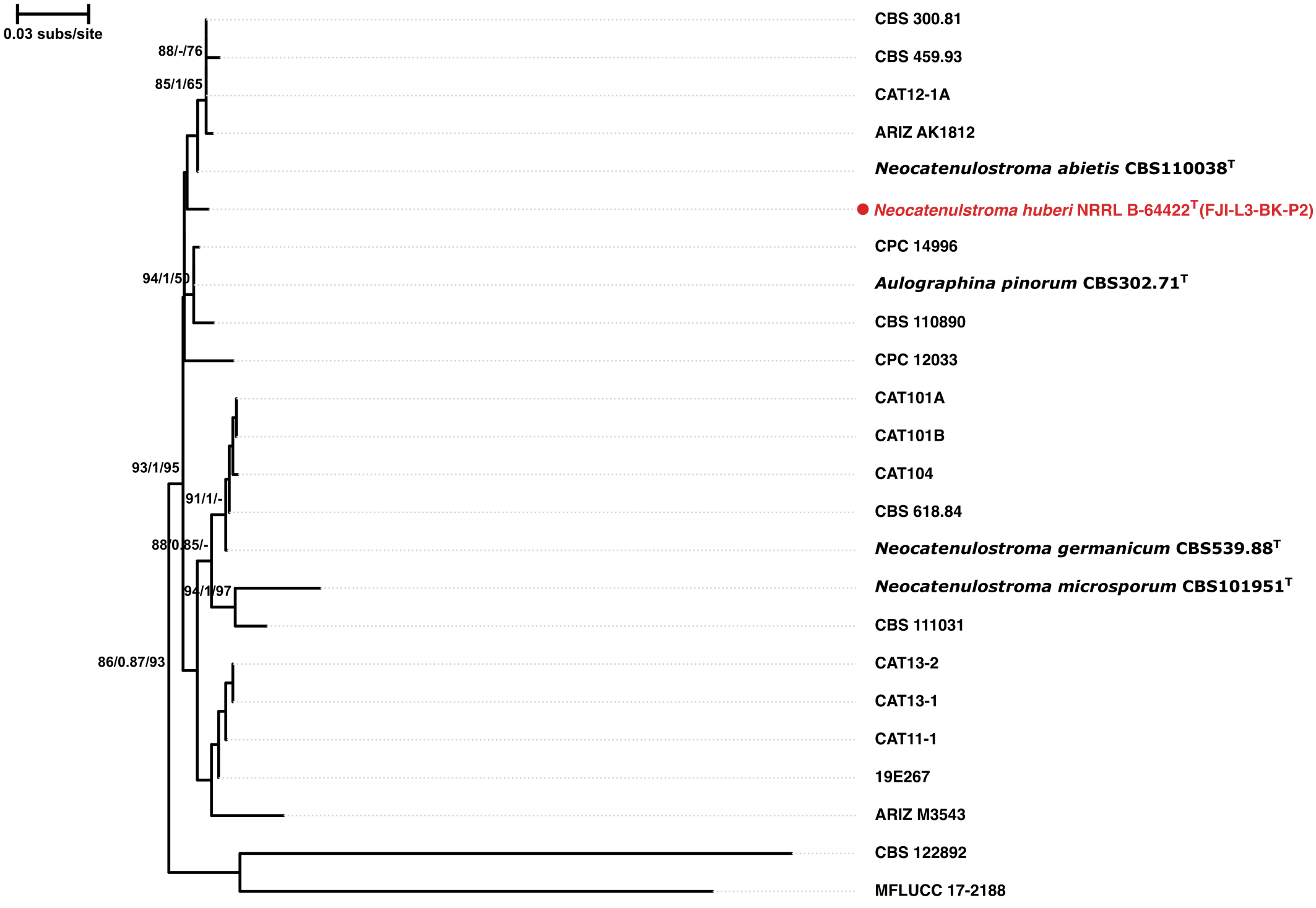
Phylum
Ascomycota

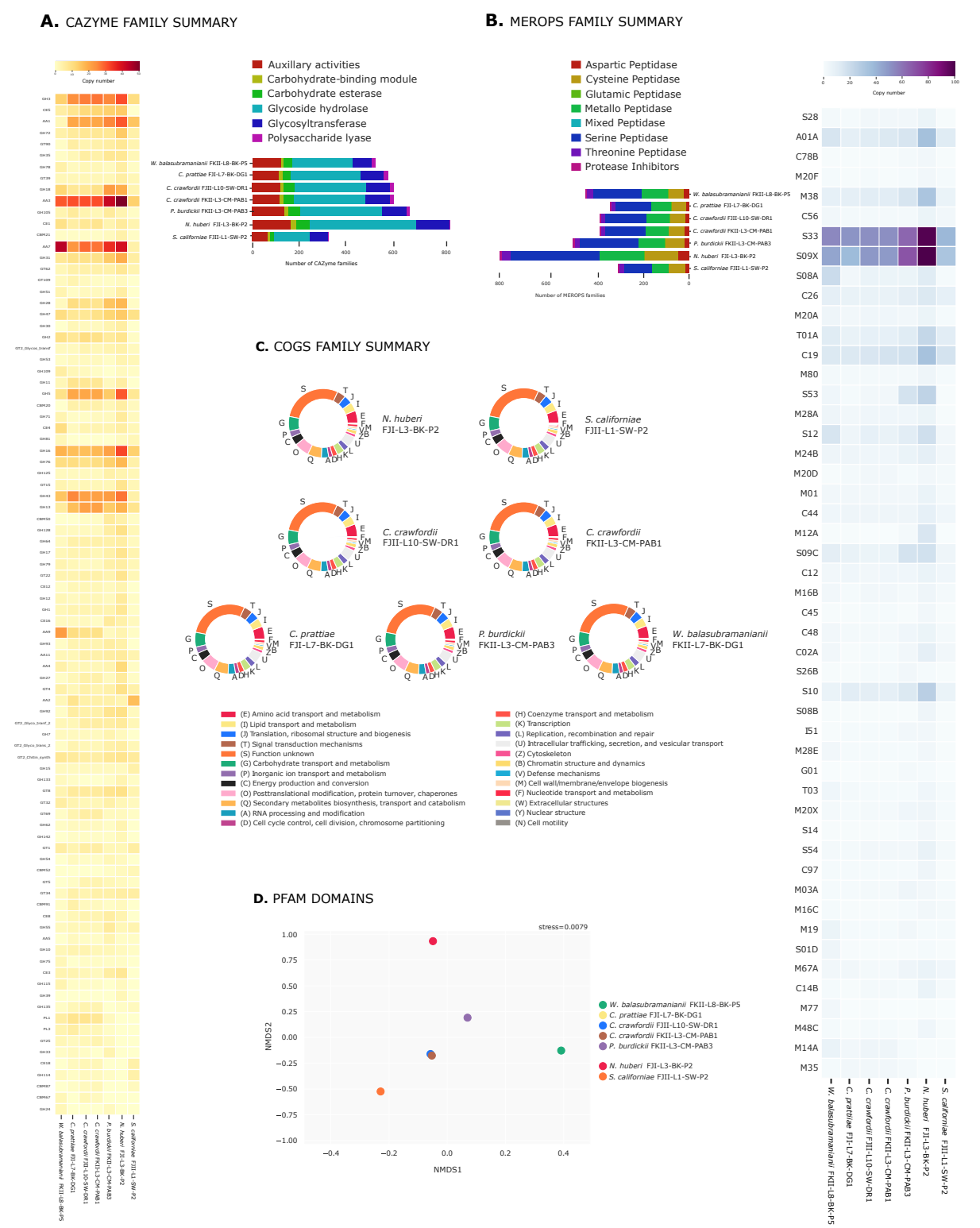

0.03 subs/site
100/1/100
100/1/100
93/1/84
96/1/95
92/1/87
I
II
III
IV
V
SFC20230103-M03
JZB390056
SFC20230103-M02
SFC20230103-M04
SFC20230103-M05
CPC 22331
CPC 22297
JZB390057
GUCC 401 6
CPC 22328
CPC 22329
Cladosporium crawfordii NRRL B-64425T(FKII-L3-CM-PAB1)
CPC 22327
DTO 127-E2
SM1
SM4
DTO 323-E8
DTO 324-D1
DTO 324-A6
DTO 324-A2
CMG 46
DTO 323-E9
CPC 14247
CPC 12216
GP20-28
GP20-29
DTO 323-E4
SFC20230103-M25
SFC20190416-M01
SFC20230103-M26
KUC1767
Cladosporium perangustum CBS 125996T
KUC1462
CPC 13870
CPC 22375
CPC 11819
CPC 11831
CPC 11821
CPC 11663
CPC 11815
CBS 126365
CPC 22378
DTO 127-E1
CPC 13730
CPC 13774
CPC 13727
CPC 15192
CMG 44
Cladosporium xanthochromaticum CBS 126364T


0.05
Waltergamsia mali ACCC 39305T
Waltergamsia pilosa CBS 124.70T
Waltergamsia fusidioides CBS 840.68T
Waltergamsia parvae CBS 381.70AT
Waltergamsia citrina CBS 384.96T
Waltergamsia hennebertii CBS 768.69T
Waltergamsia maroccana CBS 512.82T
Waltergamsia balasubramanianii NRRL 64428T(FJI-L3-BK-P2)
Waltergamsia alkalina CBS 741.94T
Waltergamsia yunnanensis GZCC 23-0746T
Waltergamsia obpyriformis CBS 595.73T
Waltergamsia catenata CBS 102462T
Waltergamsia harwoodiae MST FP3578T
Waltergamsia zeylanica CBS 735.73A
Waltergamsia epimycota CBS 562.86
Waltergamsia dimorphospora CBS 139050T
Waltergamsia mpumalangana CBS 150065T
Amphichorda cavernicola CGMCC 3.19571T
Amphichorda felina CBS 250.34
Amphichorda felina CBS 648.66
Stephanonectria chromolaenae MFLUCC 18-0589T
Stephanonectria keithii CBS 100007
Sesquicillium candelabrum CBS 119045T
Clonostachys buxicola CBS 102419T
Clonostachys rhinolophicola KUMCC 21-0439T
Tilachlidium brachiatum CBS 505.67
Tilachlidium brachiatum CBS 363.97
Sesquicillium cavernum CV00218T


0.10 subs/site
74
99
100
62
17
53
22
72
65
66
P. scytalidii CBS 118493 CPC 10998T
P. stramenti CBS 118909 CPC 11545T
P. eugeniicola CPC 2557T
P. eugeniae CPC 15143 CBS 142184T
P. pteridivora CPC 24683 COAD 1182T
P. burdickii NRRL 64430T(FKII-L3-CM-PAB3)
P. concentrica CPC 3615T
P. indica CBS 157.75T
P. eucalypticola CPC 26523 CBS 141294T
P. vochysiae LGMF 1215T
P. hymenocallidicola CPC 25014 CBS 139912T
P. hymenocallidis CPC 25018 CBS 139911T
L. acicola CBS 133791 WPF13.12T


0.20 subs/site
97
100
100
100
100
100
100
99
96
S. ramosus CGMCC 3.17076T
S. ramosus CGMCC 3.17075
S. ramosus CGMCC 3.17077
S. aggregatus CGMCC 3.17073
S. aggregatus CGMCC 3.17074
S. aggregatus CGMCC 3.17072T
Dothideomycetes sp. CGMCC 3.17079
Dothideomycetes sp. CGMCC 3.17080
N. floridanus CPC 45908 CBS 152209T
S. endophytica SDBR-CMU319
S. californiae NRRL 64432T(FJII-L1-SW-P2)
Dothideomycetes sp. CGMCC 3.17078
Dothideomycetes sp. DVA4
Dothideomycetes sp. DVA7
A. megaspermum AFTOL-ID 2094T


0.03 subs/site
88/-/76
85/1/65
94/1/50
93/1/95
91/1/-
88/0.85/-
94/1/97
86/0.87/93
CBS 300.81
CBS 459.93
CAT12-1A
ARIZ AK1812
Neocatenulostroma abietis CBS110038T
Neocatenulstroma huberi NRRL B-64422T(FJI-L3-BK-P2)
CPC 14996
Aulographina pinorum CBS302.71T
CBS 110890
CPC 12033
CAT101A
CAT101B
CAT104
CBS 618.84
Neocatenulostroma germanicum CBS539.88T
Neocatenulostroma microsporum CBS101951T
CBS 111031
CAT13-2
CAT13-1
CAT11-1
19E267
ARIZ M3543
CBS 122892
MFLUCC 17-2188


A. CAZYME FAMILY SUMMARY
Copy number
Auxillary activities
Carbohydrate-binding module
Carbohydrate esterase
Glycoside hydrolase
Glycosyltransferase
Polysaccharide lyase
W. balasubramanianii FKII-L8-BK-P5
C. prattiae FJI-L7-BK-DG1
C. crawfordii FJII-L10-SW-DR1
C. crawfordii FKII-L3-CM-PAB1
P. burdickii FKII-L3-CM-PAB3
N. huberi FJI-L3-BK-P2
S. californiae FJII-L1-SW-P2
Number of CAZyme families
B. MEROPS FAMILY SUMMARY
Aspartic Peptidase
Cysteine Peptidase
Glutamic Peptidase
Metallo Peptidase
Mixed Peptidase
Serine Peptidase
Threonine Peptidase
Protease Inhibitors
Number of MEROPS families
Copy number
S28
A01A
C78B
M20F
M38
C56
S33
S09X
S08A
C26
M20A
T01A
C19
M80
S53
M28A
S12
M24B
M20D
M01
C44
M12A
S09C
C12
M16B
C45
C48
C02A
S26B
S10
S08B
I51
M28E
G01
T03
M20X
S14
S54
C97
M03A
M16C
M19
S01D
M67A
C14B
M77
M48C
M14A
M35
C. COGS FAMILY SUMMARY
N. huberi FJI-L3-BK-P2
S. californiae FJII-L1-SW-P2
C. crawfordii FJII-L10-SW-DR1
C. crawfordii FKII-L3-CM-PAB1
C. prattiae FJI-L7-BK-DG1
P. burdickii FKII-L3-CM-PAB3
W. balasubramanianii FKII-L7-BK-DG1
(E) Amino acid transport and metabolism
(I) Lipid transport and metabolism
(J) Translation, ribosomal structure and biogenesis
(T) Signal transduction mechanisms
(S) Function unknown
(G) Carbohydrate transport and metabolism
(P) Inorganic ion transport and metabolism
(C) Energy production and conversion
(O) Posttranslational modification, protein turnover, chaperones
(Q) Secondary metabolites biosynthesis, transport and catabolism
(A) RNA processing and modification
(D) Cell cycle control, cell division, chromosome partitioning
(H) Coenzyme transport and metabolism
(K) Transcription
(L) Replication, recombination and repair
(U) Intracellular trafficking, secretion, and vesicular transport
(Z) Cytoskeleton
(B) Chromatin structure and dynamics
(V) Defense mechanisms
(M) Cell wall/membrane/envelope biogenesis
(F) Nucleotide transport and metabolism
(W) Extracellular structures
(Y) Nuclear structure
(N) Cell motility
D. PFAM DOMAINS
stress=0.0079
NMDS1
NMDS2
W. balasubramanianii FKII-L8-BK-P5
C. prattiae FJI-L7-BK-DG1
C. crawfordii FJII-L10-SW-DR1
C. crawfordii FKII-L3-CM-PAB1
P. burdickii FKII-L3-CM-PAB3
N. huberi FJI-L3-BK-P2
S. californiae FJII-L1-SW-P2

Supplementary Files

This is a list of supplementary files associated with this preprint. Click to download.

- Table2genomiccharacteristicsFINAL.xlsx
- Table1MLSAsequencecomparisons.pdf
- 03.SupplementalFilesTextandTables.pdf